Modelling Charge Transport in Organic Semiconductors

Daniels, Alex

Award date:
2017

Awarding institution:
University of Bath

Modelling Charge Transport in Organic Semiconductors

Alex Edward Daniels

A thesis submitted for the degree of Doctor of Philosophy

Department of Physics
University of Bath

27th March 2017

Copyright

Declaration

I hereby declare that this thesis has not been and will not be submitted in whole or in part to another institution for the award of any other degree.

Signature: 

Alex Edward Daniels

Acknowledgements

PhD's are tough... really really tough, but with the right people around you those tough times don't seem so bad. I have been lucky enough to be surrounded by people throughout my PhD who have supported me to no end. Three people in particular especially deserve my thanks as I'm fairly certain without them I would never have made it to this point.

The first of these people is my loving girlfriend Scarlett. Without doing this PhD I would never have met her and that in itself makes going through this process seem all the more worthwhile. Her support and encouragement throughout the last year, along with her own enthusiasm for life, has shown me what lies ahead of me in life and this has motivated me more than I thought were possible.

The second person has to be the one and only Alexander 'Smithy' Smith who, having joined our group halfway through my PhD, has done the best he can to keep me on straight and narrow when it comes to the work side of things. I feel honoured to have worked alongside someone who is not only incredibly dedicated to their own work, but also in making sure all those around them succeed too. On top of being a very insightful scientist he is also one of the most genuinely nice guys I have ever met.

The final of the three is one of my longest standing friends Iain Templeman, who has not only supported me during the PhD, but also did the same throughout my undergraduate studies. The reason as to why he has put up with me for this long already I will never know! I'm really going to miss our weekly social gaming evenings/random rantings about everything that is wrong with the world!

Of course there are many other people that deserve my thanks as well as those three. To my other closest friends Adam, Chris, James and Tom, I have thoroughly enjoyed all the times we have spent over the years, even if at times the conversations may have gone further south than the south pole (I'm looking at you in particular Tom :P). To those I have worked alongside when teaching at the university (in particular Ashley, Jenny and Isobel), I have learnt so much from you all and am really going to miss working with you all!

Also without the support of my family I would never have gotten to university in the first place. To my parents, John and Tracey, I cannot thank you enough for being there whenever I need anything. You have always encouraged me to be the best I can be and I can only hope that I have made you proud with how I have led my life so far. I am also lucky enough to still have two sets of loving grandparents who are always on the end of the phone when I need to talk.

Finally I need to thank those who have given me the opportunity to take on this task. The first and foremost of these is Professor Alison Walker, who hired me, has put up with me when I've been a nightmare to deal with, and has gotten me through to the end of this process. Secondly is Stephen Wells, whose original concepts led to the creation of this project and who has always done his utmost to try and make sure it succeeds. Finally David Sparrowe, who as an industrial supervisor, has provided support both financially and academically.

Acknowledgement of Collaboration

As the work undertaken in this PhD was such a vast area of study there were sections in which collaboration was necessary in order to complete the body of work within the required amount of time, therefore this section highlights specifically where work was performed by other parties during the PhD.

Alexander Smith directly collaborated on a large portion of the work in the last year of the PhD as he is the direct successor of the project. His contributions consisted of the co-development of the ellipsoid intersection logic and also the development of the minimum volume enclosing ellipsoid code. Additionally he also primarily undertook the translation of the FRODA code from C# to C++.

Ian Thompson developed the Mesh Kinetic Monte Carlo model used for the charge transport calculations and also provided support with the development of the minimum volume enclosing ellipsoid code.

Abstract

The search for energy efficient materials is more important now than it has ever been before. As such, computational models that investigate charge transport properties of materials have grown into an incredibly vast field of research. These models require knowledge of the structures that materials form, along with their electronic structure characteristics.

The primary focus of this work was to develop a model, based on an existing model used for investigating protein structures, that would allow for a large number of molecular morphologies to be generated. This model allows for a full atomistic morphology to be generated (which is important for charge transport simulations) at a fraction of the computational cost of conventional techniques by treating molecules as a series of rigid sections.

The model has been validated using two well documented test case morphologies, the first, Buckminsterfulerene due to its spherical nature, and the second, hexane due to its flexibility. After validation the model has been used to generate morphologies for a subset of dithiophene derivatives that our industry sponsor was interested in. Charge transport simulations were then performed on these morphologies and these are the key result of this research. We have shown clear trends in how varying the composition of the sidechains of these dithiophene based molecules directly affects the mobilities they exhibit and thus, that charge transport is incredibly sensitive to morphology.

Contents

List of Figures

Chapter 1

Introduction

The search for novel materials that are efficient at energy generation has grown in significance greatly in recent years. The desire to harness solar energy, or make electronic components found in most modern devices, has led to a vast field of research, both theoretical and experimental. Examples of the experimental work include developing organic thin film transistors (OTFTs) and organic light emitting diodes (OLEDs). OTFTs and OLEDs are of particular interest as they are low cost and are more adaptable, for example, they can be produced on flexible substrates, making them ideal for implementation in new technologies[1]. This research focuses on the theoretical arm of the field. The need for theoretical predictions in this area is important as the number of possible molecules that can be used for various applications is large, and thus, manufacturing all of them to test is not feasible. The benefits of theoretical predictions are abundant; the cost of simulating a material is generally much lower than of manufacturing it into a device. The time taken to simulate charge transport properties of materials will normally be shorter than that of the manufacturing and testing process. It is possible to investigate many materials simultaneously through theoretical predictions, this

is only limited by available computing power. Theoretical predictions, do however, have their drawbacks; simulation methods require approximations, sometimes due to the limitations on memory available to the computer, and in other times to increase the efficiency of the simulation. This can lead to some errors in the final properties of a material, however, the simulations give a good indication as to what materials it is worth manufacturing even with these approximations.

The primary aim of this research was to calculate the charge transport properties for organic materials based on their molecular structure. Charges in disordered organic films are localised at room temperature due to the electronic configuation of organic molecules and the charge transport mechanism is the hopping between the localised areas of charge. This research could therefore be broken down into three tasks. The first was how to generate morphologies for the materials that were being investigated. This is the main focus of the research and the most difficult of the three tasks. The morphology generation is very important as charge transport is very sensitive to molecular packing. The relative distance and orientation between molecules can have drastic effects on the efficacy of charge hopping rates and thus finding the correct packing for a system is crucial to finding the correct charge transport properties. The second problem was how to calculate the charge hopping rates between sites. As stated before, the orientation and distance between neighbouring sites has a large effect on the charge coupling between them. Therefore calculating these rates in a sensible manner is also very important. The final problem was to calculate the overall charge transport properties, specifically the charge mobilities, of the materials being investigated. This was achieved using a Kinetic Monte Carlo simulation, a staple of our research group and an incredibly versatile simulation technique.

Overall the key achievement of this research is the bringing together of some well known techniques, such as quantum chemistry methods for calculating charge coupling and kinetic Monte Carlo for a time-based simulation of charge transport, along with some more novel and lesser known techniques, primarily the Framework Rigidity Optimised Dynamic Algorithm (FRODA) for the morphology generation, and some novel ideas on improvements to these methods in order to create a method of calculating the charge transport of a material from its atomic structure alone. This has led to theoretical modelling of a class of dithiophene molecules which had not been investigated before and has resulted in predictions of the effect varying the sidechain groups on these molecules can have on their transport properties.

As stated initially, this is a vast field of research, and as such, there are many other techniques currently being employed to try and tackle the problems above. Examples include various forms of Molecular Dynamics for morphology modelling, many variations of density functional theory calculations for the charge hopping rate calculations, and drift diffusion models are used on larger scales to give device characteristics for charge properties. A full look into these and other methods will be covered later in the literature review.

Chapter 2

Current Methods in Morphology Generation and Charge Transport

Research into charge transport in organic materials can be traced back as far as the late 1960s [2][3]. These examples focused on analytical approaches to evaluating mobilities in known simple structures through computational means, however, as the field has progressed more sophisticated techniques have been developed to deal with more complex systems. The reasons this area has continued to grow throughout the years, are twofold. The first is that the growing need for energy efficient materials to be developed at low cost to manufacturers means that computational models are essential. The second is that as computational processing power has increased, the development of more complex models that can deal with larger systems has become possible. To give and indication of the extent of research that is present in the area of charge transport of organic materials, a simple literature search reveals a drastic increase in the number of papers over the past ten years.

As stated before, this work falls into three areas and as such this literature review will discuss the various techniques currently used in these three areas along with work that has already contributed to the techniques we are employing.

2.1 Morphology Generation

There are currently many techniques employed to investigate morphologies of molecular systems. The most common branch of these start with the foundations of molecular dynamics. Molecular dynamics simulations of this nature can be dated back as far as the late 1950's when Alder and Wainwright [4] first employed the methods as a direct competitor for statistical mechanics. A key example of the statistical mechanics simulations to which molecular dynamics was orignally competing with is that of Edwards [5]. Edwards investigated the configurations of polymers by treating them as freely hinged links under the influence of a self-consistent field. He highlighted the limitations of this method, the key one being that computing first approximations of the self-consistent field is straightforward, however, higher approximations require so much computing power that it is virtually impossible. The molecular dynamics simulations are computationally expensive as they rely on forces to be calculated for all interactions between atoms in a system [6], but not to the same extent as the statistical mechanics simulations. As such, in recent years, a lot of work has gone into researching coarse graining techniques, where clusters of atoms, or in some cases entire molecules, are grouped together and treated as one entity. This reduces the total number of interactions in the system, but the results are highly dependent on how the groups of atoms are clustered. The first of these coarse grained models

was a simplification of a polymer chain shown by Baschnagel et.al. [7]. As the field has progressed, more sophisticated methods of coarse graining have been developed, and at the forefront of these are those researched by Zannoni et.al [8][9][10].

Molecular dynamics is a useful tool as, with the correct choice of potential, it can be used to accurately simulate atomic motion. This does not mean, however, it is without its drawbacks. As stated previously, it is a very computationally intensive technique and as such it is not always practical, even with the recent developments in coarse graining, to use on device scale size systems.

Monte Carlo simulations are another method of morphology generation techniques that once again started from simple models. As with all Monte Carlo methods the premise is to design a model in which at some point a random element can be introduced. Normally this random element is based on the assumption that a process that reduces the energy of a system should always be accepted, but otherwise there is a random chance of acceptance. The earliest of these methods for morphology generation can be seen in Verdier [11] which attempts to simulate a simple polymer chain of varying sizes. These methods have expanded to more complex systems, such as those of the polymers seen in Guttman and DiMarzio [12]. In more recent years sophistcated methods such as those seen in Diani and Gilormini [13] have been able to show glass transition effects within polymer systems.

As with molecular dynamics, Monte Carlo simulations have also proven to be useful in many areas of physics. Monte Carlo simulations tend to be less computationally intensive than their molecular dynanics counterparts and thus can deal with larger systems, however, due to the random nature of the simulations the selection of parameters can have a drastic effect on the

results produced. Monte Carlo simulations of morphology generation work on the premise that physically realistic structures can be found through non-physical moves[14].

Deciding between whether to use a molecular dynamics simulation or a Monte Carlo simulation is dependent on what type of system is being investigated and what timescales the evolution of these systems need to be explored over. Molecular dynamics is a more physical approach to finding morphologies, however, it can only run over very short timescales of the order of nanoseconds. Monte Carlo on the other hand can explore moves that would not be practical to explore with molecular dynamics, but requires a lot of care and thought to go into developing the moves used.

Both Monte Carlo and molecular dynamics simulations have been used in conjunction with each other as complementary techniques. This has primarily been achieved in two ways, the first, running independent simulations using both methods and comparing the results from each [15][16][17]. The other, using Monte Carlo simulations to generate sensible starting points for molecular dynamics simulations, or introducing Monte Carlo steps into the molecular dynamics simulations, thus reducing the length of the computationally intensive molecular dynamics part of the simulation [18][19][20].

The model that this work focuses on is an adapted version of Wells et al. Framework Rigidity Optimised Dynamic Algorithm (FRODA)[21] (in which a full outline of the methods is present in chapter 3), an alternative to molecular dynamics and Monte Carlo simulations which is less expensive computationally than molecular dynamics, however, uses a more physical moveset than Monte Carlo simulations. The work on this model currently has been focused around investigating protein flexibility using methods developed from Wells' previous work [22] along with previous work on protein analysis

such as the anisotropic network model [23][24][25]. One of the key aspects of this methodology is the rigidity analysis applied to chemical structures [26]. The methodology has been developed over recent years to investigate how the normal modes of motion that are defined by low frequency phonon modes, allow the large conformational space available to proteins to be explored [27]. This has led to explanations of biological phenomena, such as crosslinking of specific regions in proteins, being attibuted to the rigidity of the protein [28] and also how rigidity/flexibility is key to certain biological processes that proteins exhibit [29]. The work to this point is outlined well in Wells' chapter in "Protein Dynamics"[30] covering the new methodology that had been developed to investigate various protein structures, which in itself shows the method is a powerful tool. Most recently the method has been expanded to deal with not only proteins but also metal-organo frameworks [31] which gives a good foundation for these methods to be used to explore organic semiconductors. The methodology has also been shown to compare well with molecular dynamics simulations [32][33].

2.2 Charge Hopping Rates

There are two methods of calculating charge hopping rates, Miller-Abrahams rates and Marcus rates, that are the most common. The first of these methods is a more approximate method, but is commonly used, and was originally introduced by Miller and Abrahams in 1960 [34]. Miller-Abrahams tends to find more prevalent use in systems in which orientation is less of an issue such as lattice based morphologies [35]. The other common method is the use of Marcus rates, which relies on the calculation of transfer integrals between charge hopping sites [36]. As such this method requires more complex

parameters to be calculated in advance, however it does allow for orientation of charge hopping sites to be accounted for.

Marcus rates,

$$k_{et} \approx \frac{2\pi}{\hbar} \frac{|V|^2}{(4\pi\lambda k_B T)^{\frac{1}{2}}} e^{-\left(\Delta G^0 + \lambda\right)^2 / 4\lambda k_B T} \tag{2.1}$$

where k_{et} is the hopping rate for electron transfer, V is the transfer integral, λ, the reorganisation energy, ΔG^0, the Gibbs free energy of reaction, $\hbar$ is the reduced Planck constant, k_B is the Boltzmann constant and T the absolute temperature, directly require the calculation of the transfer integral as this determines the maximum hopping rate.

Charge transfer is a vast area of research that has branched off from that of investigating electron orbitals and it is important to note here the various methods that are used to calculate these integrals. The foundations of these methods primarily come from Hohenberg, Kohn and Sham's development of density functional theory [37][38] and the addition of excited states of electron orbitals to these methods developed by Theophilou [39], Valone and Capitani [40], Katriel [41] and Görling [42].

The first validated calculations for transfer integrals by means of DFT methods arose in 2005 as seen in Sakiyama et al. [43] and there is a large amount of published work since then which has investigated the effects molecular structure have on electron transfer properties [44] [45] [46].

2.3 Charge Transport Calculations

The key literature focussing on charge transport simulations in organics fall into three major branches, those of drift diffusion models, solutions to the master equation and Monte Carlo models. Groves [47] provides an interesting

review which highlights the key work in these areas.

Starting with the drift diffusion models, most of the work in developing these methods comes from solving the current flowing through inorganic devices, and this has recently been translated into organics [48][49]. The models have been shown to have good agreement with experimental results [50][51], however, the method is not without limitations. Analytical expressions for charge generation and recombination are required and the choice of solution used can have a significant effect on the results when modelling organic materials [52][53]. Drift diffusion models also rely on materials being described as homogeneous which in the case of organics, which exhibit energetic and morphological disorder [54][55] and therefore more detailed atomistic methods normally give more accurate results.

The Pauli master equation [56] led to a charge transport model that uses charge hopping rates allowing three dimensional charge transport to be described as a continuum throughout a material. This allows for much faster simulations than the alternative methods [57], however, makes it difficult to account for Coulomb interactions, which is important for high charge density (around 10% of sites being occupied) situations [58][59]. Additionally when extended into three dimenisions the calculations become far less efficient. This is not to say that as a method it is inappropriate due to the approximations that are made, and it has been shown to be quite successful when applied to predicting organic device characteristics [60][61].

The final branch of charge transport simulations is that of the Monte Carlo simulations, which come in two separate forms, kinetic Monte Carlo, where random events are based on rates and a system time is introduced, and quantum chemical Monte Carlo, an extension of the kinetic Monte Carlo method which requires the quantum chemical properties of a material to be

stated explicitally in order to generate the hopping rates. For our purposes a Monte Carlo simulation will be used and the justification for this will become apparent. Monte Carlo is an area of research we are quite familiar with as various models have been developed within our research group [62][63]. There are many implementations of kinetic Monte Carlo simulations and specifically in our group we use the first reaction method, in which the time until an event occurs is randomly generated based on the the inverse of the rate of that specific event. After all possible event times have been generated, they are sorted and the event with the shortest execution time is performed.

As with all Monte Carlo simulations, the key part is a random element biased in some statistical manner. In the case of charge transport the random element comes with the rate at which charges hop. One of the major benefits to using Monte Carlo methods over drift diffusion or the master equation is that it is implemented as a particle to particle model, but also provides device characteristics, thus bridging the gap between atomistic and continuum models. Additionally, it becomes possible to treat site coordinates as continuous rather than each site being requied to sit on a lattice point [47]. This does lead to large numbers of calculations being required to determine hopping rates, which is described above in §2.2. However, when it comes to organic devices, morphological disorder is commonplace [47]. As such, Kinetic Monte Carlo simulations are ideal for charge transport in organic devices as the method allows for charges to be traced through the morphology, allowing information on trap sites and the paths that current flow through to be investigated.

It is important to state at this point that the work to be undertaken in this thesis is a bottom-up approach to studying charge transport in organic materials, and this could lead to a description of energy and spatial distri-

butions of trap sites found in these types of devices which are normally used in top-down transport calculations as in Bässler [64]. Bässler's approach is that of a time of flight model, also seen in other works such as Li [65], and is an approach in which carriers have their own local time and begin at one electrode. Whichever carrier hop would advance the global system time by the smallest amount is executed and then the potentials in the system are updated to calculate the new times. Once all carriers have reached the opposite electrode the simulation ends. This is similar to the kinetic Monte Carlo methods, however slightly less sophisticated in that it is a deterministic method due to the approximations it uses. By directly modelling the morphologies on an atomic level and using a kinteic Monte Carlo method to simulate charge flow it should be possible to explicitly find how trap sites are distributed within the morphologies.

2.4 Summary

In summary, having discussed all of the methods above, it is clear which methods are appropriate for this research. The morphology generation will be performed using an adaptation of the FRODA algorithm as it allows us to retain atomic level detail whilst not being as computationally intensive as the alternative methods discussed. The charge hopping shall be calculated by quantum chemical methods as these give us accurate hopping rates for charge carriers between hopping sites and can be tuned as necessary based on the atomic structure of the molecules being studied. Finally the charge transport calculations will be performed using a Kinetic Monte Carlo method as this allows us to trace the paths charge carriers take through our morphologies, giving the possibility of eventually being able to identify trap sites. All of

these methods are outlined in the next chapter and show significant promise in being a suitable alternative to the current methods discussed in this chapter.

Chapter 3

Theory

This chapter will focus on the underlying theory behind the methods used throughout the course of the research. The main areas to cover will be that of the morphology generation, the calculations performed to find the hopping rates of charge carriers within the morphologies and finally the theory behind the charge transport calculations that give the overall properties of the materials in question.

3.1 Morphology Generation

Generating atomic morphologies on the nanoscale is a computationally heavy task. As discussed in §2.1 various methods are currently employed to get around this issue. The methodology that was used in this research is based on that of Stephen Wells [21], an algorithm known as FRODA (Framework Rigidity Optimised Dynamic Algorithm).

3.1.1 Framework Rigidity Optimised Dynamic Algorithm

The basic premise of FRODA is that molecules can be broken down into groups of atoms that form rigid parts of their structure. The definition of a rigid section of a molecule in this situation is that the atoms in the section that vibrate thermally about their equilibrium positions are fixed with respect to each other. This therefore allows the expensive, high frequency, vibrational motion to be ignored for individual atoms whilst the low frequency harmonic motion, which dominates overall structural rearrangements, to be explored for the rigid sections[66]. This global motion is believed to be what defines molecular packing and therefore focussing computational effort on investigating these modes is key to finding the plausible macrostructures that organic semiconductors form. The reason the high frequency motion can be ignored is that it dominated local movement such as bond flexing, which is on a much shorter timescale than the motion which dominates molecular packing. As FRODA is primarily a heuristic method for exploring the conformational space of molecular systems, quantites such as temperature and pressure are not present, nor needed for the purposes of the simulation. This does mean that the systems investigated are not going to be driven towards an energy minimum. However, it is our belief that the dominant process that defines molecular packing is jamming, and as a heuristic method FRODA is well suited to exploring jammed states.

3.1.1.a Input Generation

The first step in this process is to start with a geometrically optimised molecule. This is achieved using the Gaussian09 density functional theory

software package. The choice of basis set is highly dependent on what atom species are present in the molecule[67]. Figure 3.1 shows a molecule drawn by hand and then optimised using Gaussian09.

Once a geometrically optimised molecule has been generated it must be split into rigid sections. An example of this is shown in figure 3.2. The rules for this selection are as follows[21]:

- Covalent bond angles and lengths must remain the same.
- Covalent double bonds cannot be rotated.
- (Optional) A series of atoms along a single bonded chain can be made rigid up to a given length (i.e. long side chains can be made more rigid to improve computational efficiency with a minor loss in accuracy).
- (For polymers) "Tethers" are formed between successive monomers to reduce the torsional flexibility of the overal chain. These essentially act as a reverse steric interaction between atoms in neighbouring monomers and ensure that a polymer chain cannot twist into an unphysical state.

With the optimised molecule now split into rigid sections it is necessary to create an input morphology. There are many ways this could be achieved however the route that was taken was to place molecules randomly, with random orientations, within a specified box size.

The first attempt to generate an input used cuboids that contained all of the atoms within the molecule. These cuboids were then placed at random one by one within the box and with each placement a check was made to see if there were any overlaps. This was achieved using the separating axis theorem for non-axis-orientated bounding boxes[68]. If an overlap was found then a new rotation of the box was attempted, and then, if after a given number of

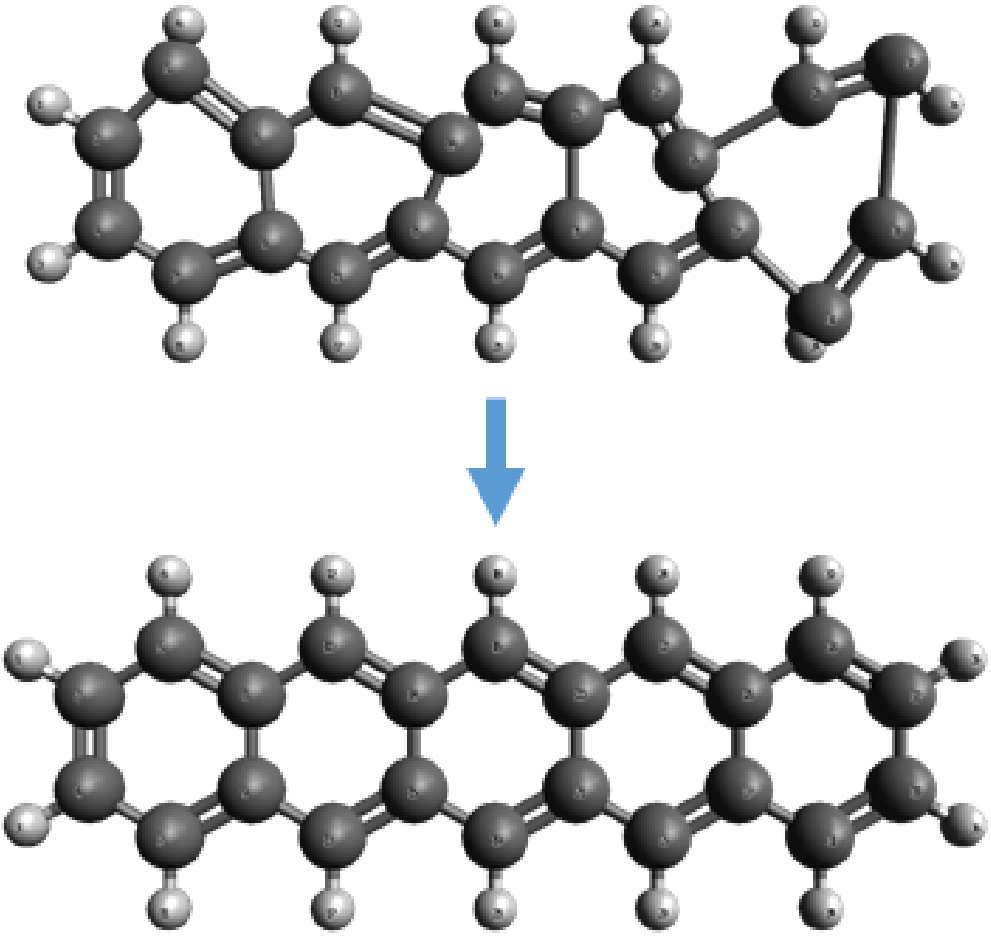

Figure 3.1: An example of the Gaussian09 geometry optimisation of a pentacene molecule. Above is the misaligned hand drawn molecule passed into the Gaussian software and below is the geometrically optimised structure produced by performing a bond energy minimisation.

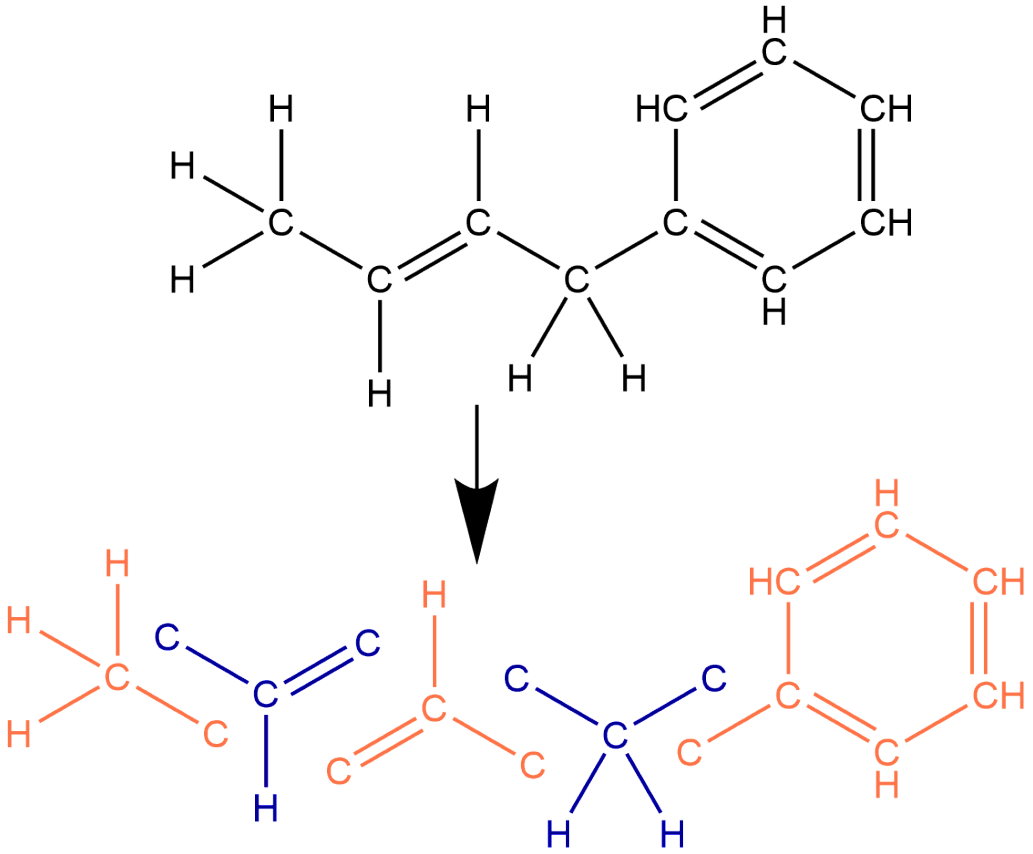

Figure 3.2: An example of the breakdown of a 1-phenyl-2-butene molecule into its constituent rigid bodies. The bodies are highlighted in alternate colours for clarity. Each neighbouring body shares a pair of atoms to ensure the bond lengths and angles remain the same as referenced by the placement of the individual bodies.

tries the box could not be placed a new centre location was chosen and the process repeated.

This method was found to have multiple problems, the largest of which being the amount of empty space each box contained due to the non cuboidal shape of molecules. Also for dense systems it was found that the algorithm could never place the required number of molecules and would end up locking up.

It was therefore decided to use a different shape for the molecules and the most logical move was for that shape to be an ellipsoid. Once again this posed more problems. The first of these was how to define an ellipsoid that contained all of the atoms within the molecule. The second was how to determine whether two ellipsoids, orientated randomly in space, intersect.

A minimising volume method was employed for the generation of the ellipsoids around molecules. This method simply shrinks a large ellipsoid down until it just contains all of the atom centres in the molecule. To ensure all atoms are contained, including their volume, six "virtual" atoms are placed one atomic radius away in each of the axes directions for each atom. From this the three principal ellipsoid axes for the molecule are found in cartesian space. These axes are then updated as the simulation moves molecules and rigid bodies in order to represent the orientation of the ellipsoid. An example of the ellipsoid generation can be seen in figure 3.3.

For the intersection between ellipsoids Alfano's method was employed[69]. This method uses an eigenvalue decomposition of the ellipsoid in a general form to determine whether two ellipsoids are separated, intersect or whether one ellipsoid completely engulfs another.

First a simple check is employed to see if the distance between the centres of the ellipsoids is larger than the sum of the two largest axes lengths. If this

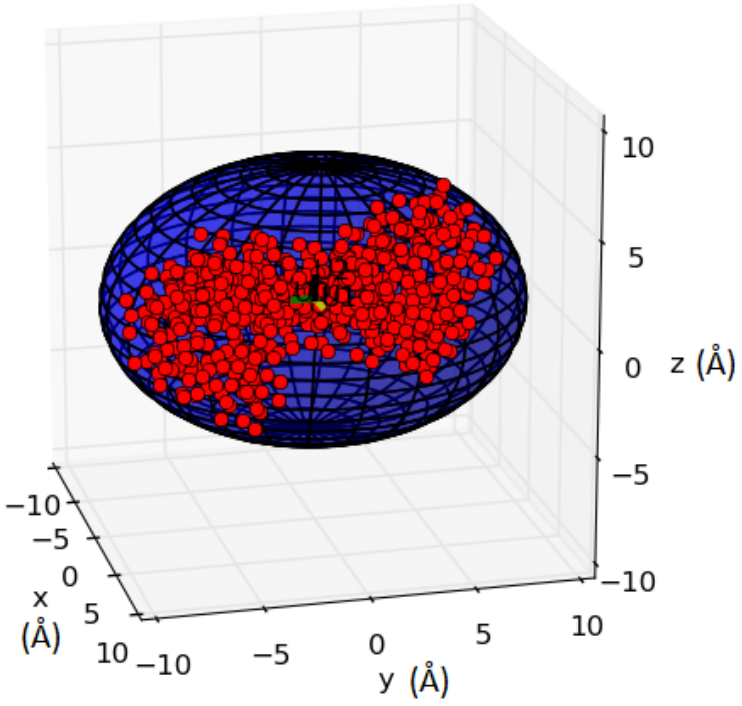

Figure 3.3: An example of the minimum enclosing ellipsoid generated for the dithiophene derivative molecule with sidechain 1 as shown in chapter 5. The red circles show the atom locations and points surrounding these that the minimum enclosing ellipsoid is fitted to.

is true then the ellipsoids cannot intersect, otherwise the eigenvalue method is employed.

The ellipsoids first need to be written in the algebraic form,

$$Ax^2 + By^2 + Cz^2 + Dxy + Eyz + Fxz + Gx + Hy + Jz + K = 0 \quad (3.1)$$

where x, y, and z are the cartesian axes, and coefficients A through K are constants that define the shape of the ellipsoid. Equation 3.1 can be written in matrix form,

$$XSX^T = 0 \quad (3.2)$$

where,

$$X = \begin{bmatrix} x & y & z & 1 \end{bmatrix} \quad (3.3)$$

$$S = \frac{1}{2}\begin{pmatrix} 2A & D & F & G \\ D & 2B & E & H \\ F & E & 2C & J \\ G & H & J & 2K \end{pmatrix} \quad (3.4)$$

These ellipsoids need to then be translated such that one of them is centred on the origin. At this point we can formulate the eigenvalue problem. If each ellipsoid is defined to be E_1 and E_2 in matrix form respectively then both ellipsoids must satisfy the condition,

$$XE_1X^T = 0 \quad (3.5)$$

$$XE_2X^T = 0 \quad (3.6)$$

If a X satisfies both of these equations then the ellipsoids must intersect. By multiplying equation 3.5 by a scalar and subtracting equation 3.6 we can

form the relation,

$$X\left(\lambda E_1 - E_2\right) X^T = 0 \tag{3.7}$$

and by selecting λ such that $(\lambda E_1 - E_2)$ is singular we can form the eigenvalue problem to solve as shown in equation 3.8.

$$XE_1\left(\lambda I - E_1^{-1}E_2\right) X^T = 0 \tag{3.8}$$

The eigenvalues found directly relate to the intersection of the two ellipsoids as shown in Alfano [69]. If two distinct negative eigenvalues are found then the ellipsoids do not intersect, otherwise an intersection has occurred, or one has engulfed the other. Due to the nature of our calculations, we are only interested in intersection or non-intersection and the engulfing case will not occur within our systems. Therefore this analytical method is ideal for our purposes.

With the addition of ellipsoids to the input generation technique, higher density starting systems were obtainable, however, the densities were still much lower than what is required for practical charge transport calculations to be performed. This can be seen in figure 3.4 by the voids that are present around the edge of the morphology, which are also present throughout the centre of the morphology too. To solve this problem two routes have been used. A compression algorithm was used within the FRODA simulation itself, this will be discussed further in §3.1.1.c. The other option was to start from an ordered structure and allow the systems to evolve into a disordered structure. The benefit to starting from an ordered structure is that it can be created at a desired density, however, there are concerns that escaping this ordered structure can be difficult, this is addressed in chapter §4. An

example of an ordered input, created by placing molecules at fixed distances in a body centred cubic like structure, is shown in figure 3.5.

With an input morphology, a geometrically optimised molecule and a list of rigid sections generated, the necessary inputs have been generated that are required to run the simulations.

3.1.1.b Moveset Generation

The first step in the simulation procedure is to generate a moveset for our rigid sections to follow. As with the proteins discussed in §2.1 an elastic modelling network is used. The network is built up of series of nodes connected together by "compressed springs" that represent the repulsive interactions through Hooke's law as in equation 3.11. These inteactions can be represented by a quadratic potential well, making a spring a logical choice as the type of interaction. The maximum cutoff distance for these interactions is determined using ellipsoid intersections for the rigid bodies using the methods described in §3.1.1.a. As we are only interested in local interactions for these bodies a cutoff size for the ellipsoids of twice the minimum volume is used. An example of the construction of a network can be seen in figure 3.6. It is important to note that the generation of the moveset does not include any information about temperature and pressure, however, the elastic modelling network has been previously proven to be a good approximation without this information.

From this network a Hessian matrix is produced of the form,

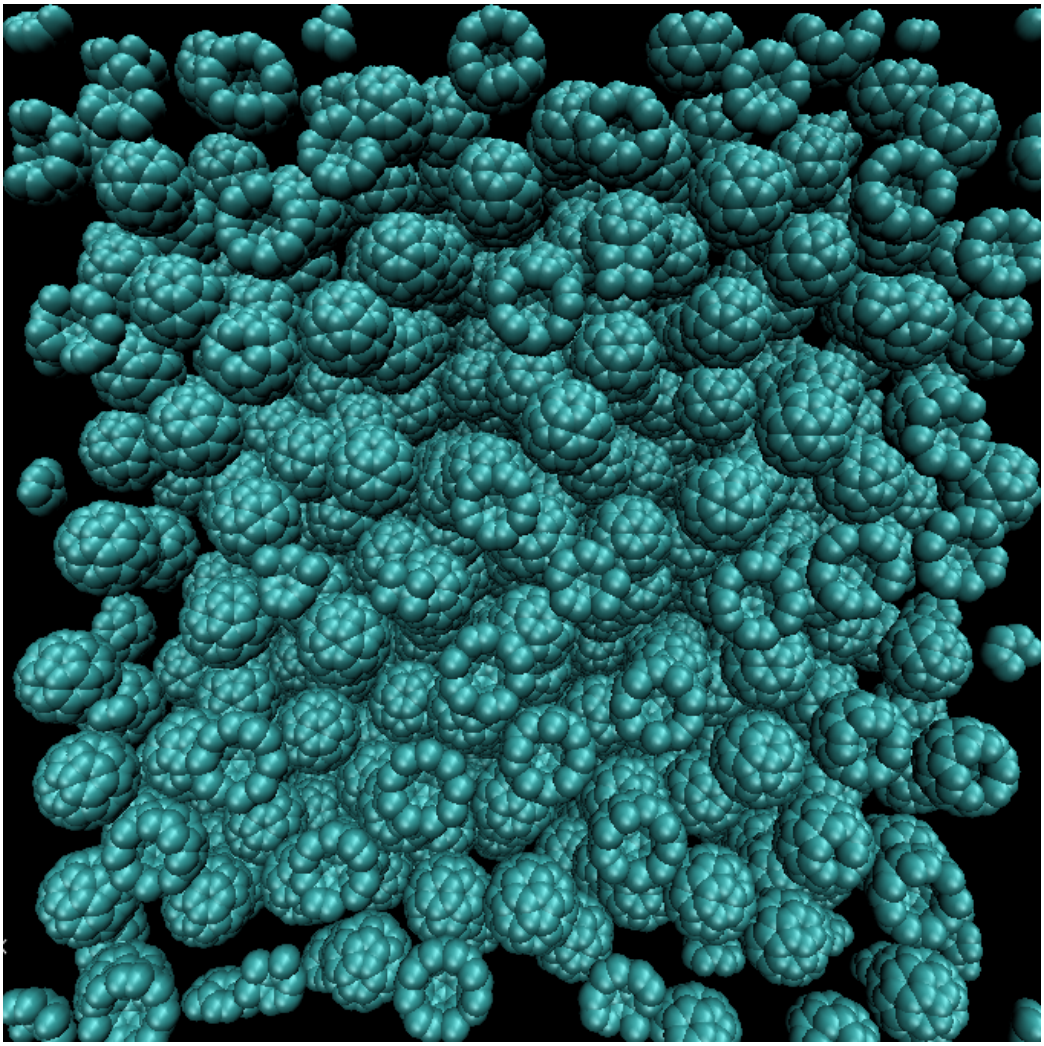

Figure 3.4: Initial random structure generated using C60, with identical ellipsoid radii of 5.3Å(as C60 is a spherical molecule), at an ellipsoid packing fraction of 0.3. The molecule fragments present at the edges of the image are due to periodic boundary conditions being applied across the cell.

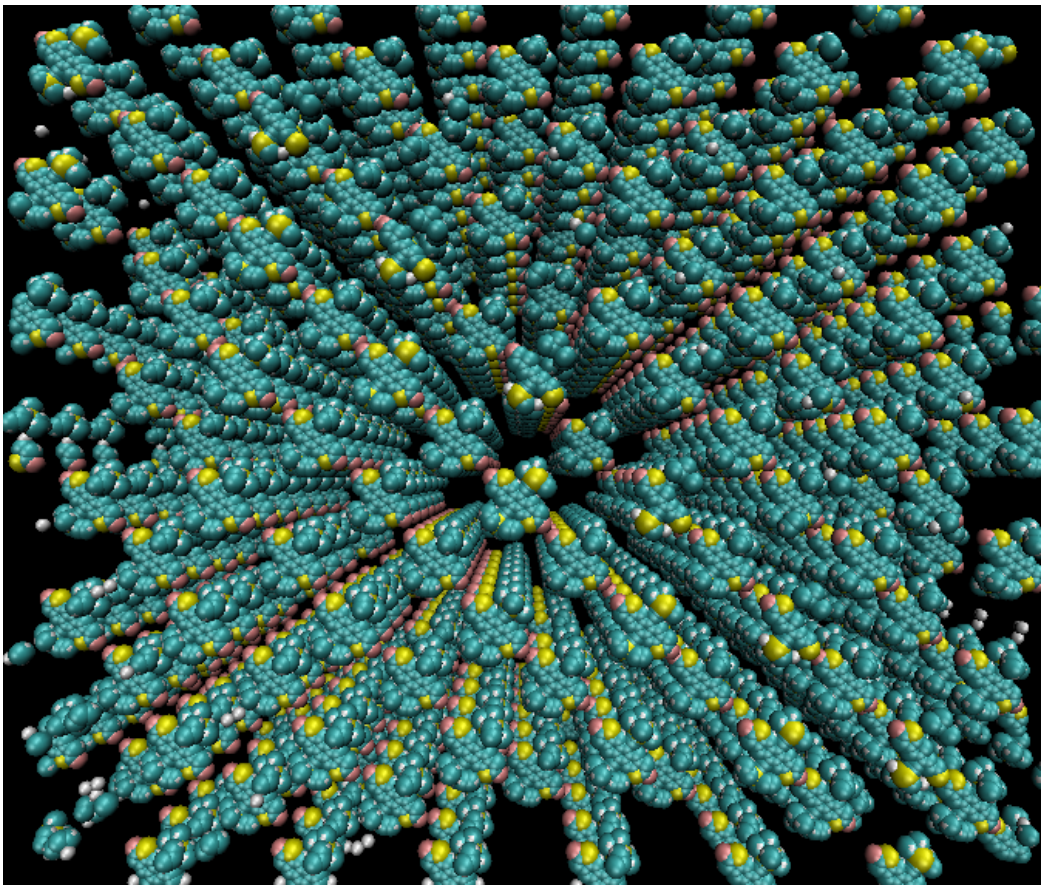

Figure 3.5: Initial ordered structure generated using an anthra[2,3-b:7,6-b]dithiophene molecule with 4,4-dimethyl-2-pentyne sidechains (as investigated in chapter 5) with spacings between molecule centres equal to twice the molecular ellipsoid radii of 10.79Å, 9.21Å and 6.03Å.

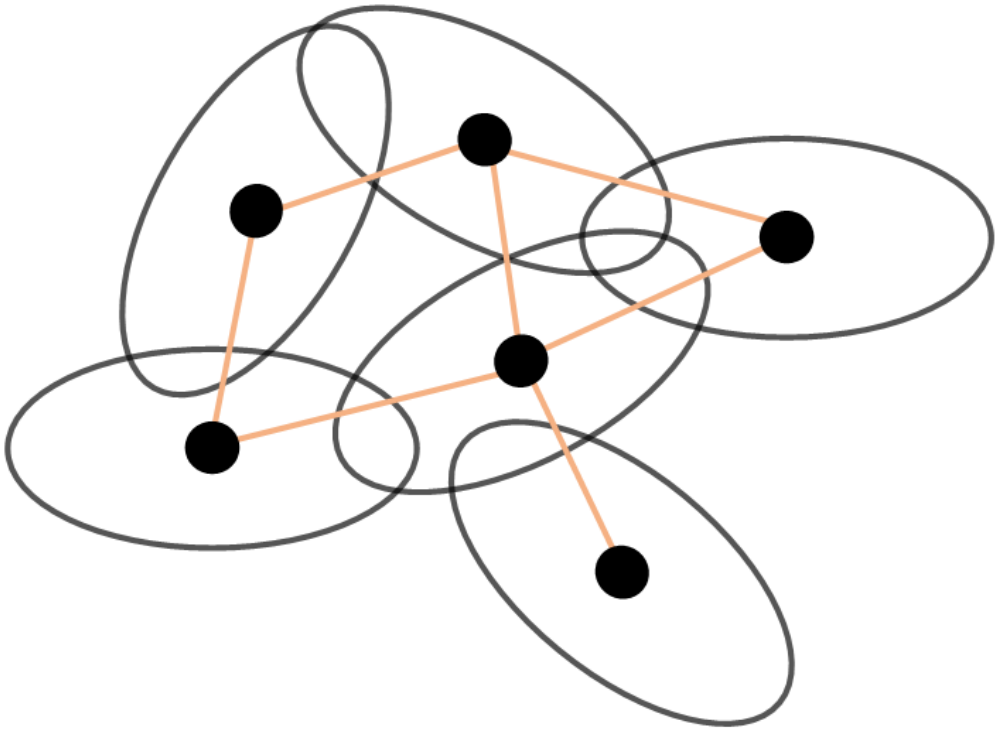

Figure 3.6: A two dimensional analogy of the type of network used in the simulations. The black circles represent rigid body centres, the ellipses surrounding them their interaction range and the lines indicating where interactions would be recorded.

$$\begin{pmatrix} H_{0,0} & H_{0,1} & \cdots & H_{0,N} \\ H_{1,0} & H_{1,1} & \cdots & H_{1,N} \\ \vdots & \vdots & \ddots & \vdots \\ H_{N,0} & H_{N,1} & \cdots & H_{N,N} \end{pmatrix} \tag{3.9}$$

where element H_{ij} is a $3x3$ super element representing the interaction of site i with site j and is of the form,

$$\begin{matrix} \frac{\partial^2 V}{\partial x \partial x} & \frac{\partial^2 V}{\partial x \partial y} & \frac{\partial^2 V}{\partial x \partial z} \\ \frac{\partial^2 V}{\partial y \partial x} & \frac{\partial^2 V}{\partial y \partial y} & \frac{\partial^2 V}{\partial y \partial z} \\ \frac{\partial^2 V}{\partial z \partial x} & \frac{\partial^2 V}{\partial z \partial y} & \frac{\partial^2 V}{\partial z \partial z} \end{matrix} \tag{3.10}$$

and the differentials are found from the potential function,

$$V = \frac{1}{2} k(\Delta x^2 + \Delta y^2 + \Delta z^2) \tag{3.11}$$

The super elements in equation 3.10 are only used for the off diagonal super elements in the Hessian, rather than represent self-interactions in the diagonal super elements, a negative sum of all other superelements in the row (or column as these are identical) are used to show the equal and opposite reaction to the interactions with other bodies and ensure the sum of the Hessian elements is equal to zero.

By finding the 3N dimensional eigenvectors corresponding to the lowest frequency non-trivial modes (that is modes which are not just translational or rotational motion of the entire system) of this Hessian matrix we gain a set of vectors that define the relative movement of each rigid body in the system along a given mode,

$$
\begin{array}{c}
Mode \\
\\
\\
\\
\\
\\
\\
\\
\\
\\
\\
\\
\end{array}
\begin{array}{c}
\begin{array}{ccccccc} 1 & 2 & 3 & 4 & 5 & 6 & 7 \end{array} \\
\begin{pmatrix}
x_0 & x_0 & x_0 & x_0 & x_0 & x_0 & x_0 \\
y_0 & y_0 & y_0 & y_0 & y_0 & y_0 & y_0 \\
z_0 & z_0 & z_0 & z_0 & z_0 & z_0 & z_0 \\
x_1 & x_1 & x_1 & x_1 & x_1 & x_1 & x_1 \\
y_1 & y_1 & y_1 & y_1 & y_1 & y_1 & y_1 \\
z_1 & z_1 & z_1 & z_1 & z_1 & z_1 & z_1 \\
\vdots & \vdots & \vdots & \vdots & \vdots & \vdots & \vdots \\
x_N & x_N & x_N & x_N & x_N & x_N & x_N \\
y_N & y_N & y_N & y_N & y_N & y_N & y_N \\
z_N & z_N & z_N & z_N & z_N & z_N & z_N
\end{pmatrix}
\end{array}
\tag{3.12}
$$

where x_i, y_i and z_i correspond to the Cartesian components of each directional movement vector.

Many solvers were tested for finding the eigenvalues and eigenvectors of our Hessian as it can be the most time consuming part of the simulation. Initially an interface with Matlab was attempted as it is a very powerful tool when it comes to matrix mathematics. Unfortunately, much as the solver itself was fast compared to other methods, the interface required writing out the Hessian to a text file for the Matlab subroutine to read in, and then once the eigenvalues and eigenvectors had been found, these had to be written out to a file for the main code to read back in. When the Hessian has large dimensions this input/output proved to be inefficient both for disk space, and the amount of time taken to read and write.

The next solver that was used was from the Math.Net C# library [70]. This solver proved to work well on small systems, however, when scaling up, was very slow to find the eigenmodes of our systems. Part of the reason

for this was the lack of ability to perform parallel processing at the time of release. This has since been resolved however a new problem presented itself in the maximum size of matrix the Math.Net library could handle.

Once the main simulation code had been converted to C++ the number of solvers available to us increased drastically. Initially the well known GSL libraries were used and proved to be quite efficient [71]. However, due to the nature of the solver it is essential to specify the full matrix and thus when reaching large system sizes the integer limit for array indices was exceeded with some of our larger systems. Also GSL calculates all eigenmodes, which given we are only interested in the smallest non-trivial modes is excessive.

At the recommendation of S. Wells an investigation of the Arnoldi method [72] was performed. This method uses a shift and invert process to approximate eigenvalues around a desired point. It then returns only these eigenvalues and eigenvectors which is ideal for our needs. Using the ARPack package along with the ARPack++[73] extension it was possible to solve systems that were taking on the order of 5 minutes to solve using GSL in under a second. Populating the Hessian takes longer than solving it using this method. Also the ARPack package has the ability to store matrices in a sparse format meaning the issues with exceeding the integer limit on array counters was also no longer an issue. Comparing the eigenvalues obtained by the different methods showed minor discrepancies due to the approximations in the Arnoldi method, however these were of the order of 10^{-5}.

3.1.1.c FRODA Algorithm

The FRODA algorithm can be broken down into three major steps that happen every simulation cycle and several optional steps as shown in the flow chart in figure 3.7.

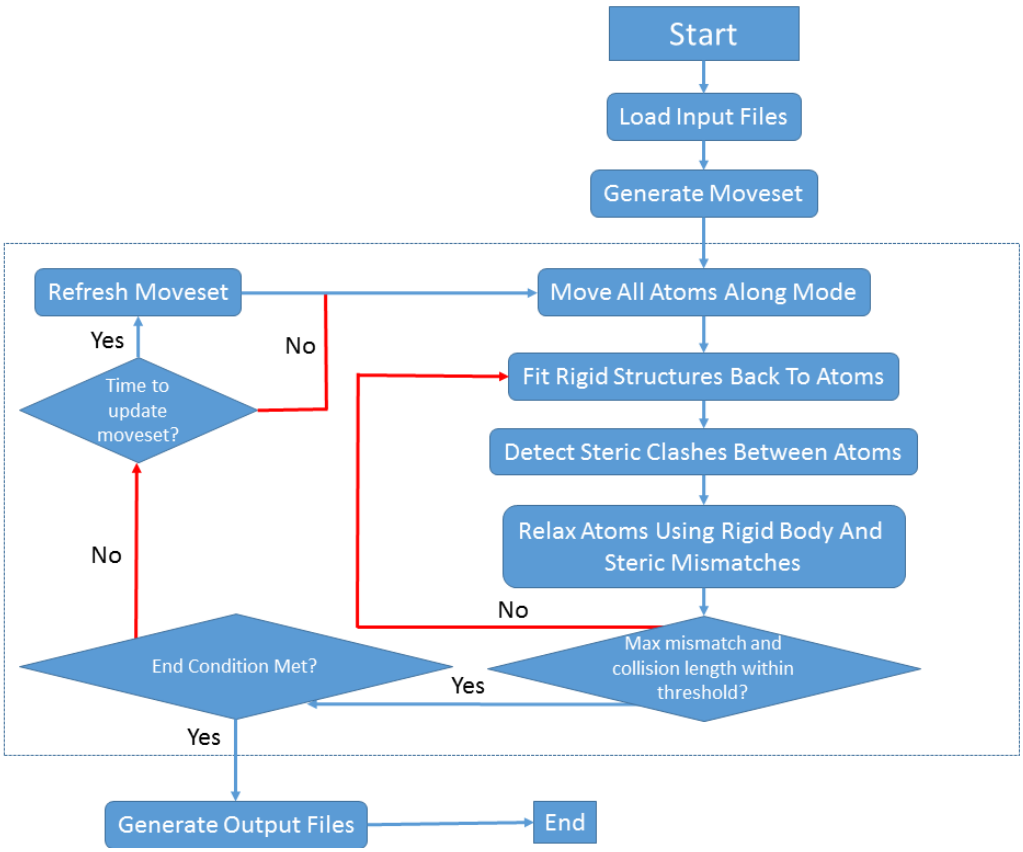

Figure 3.7: A flowchart giving the basic outline of the FRODA algorithm. Each step is discussed in full in this section.

The first step is to move all atoms in the system using the generated moveset from 3.12 by adding the individual components from each vector to the current coordinates for each atom. Atoms are moved according to the rigid structures they belong to, such that if an atom belongs to three rigid structures it will take a step in the three directions those rigid bodies wish to move in. The distance by which the atoms are moved is based on a uniformly scaled version of the selected mode, where the largest distance an atom can move can be defined as an input, typically this is taken to be 0.5Å.

Once all atoms have been moved off their rigid structures, these rigid structures have to be fitted back to the current positions of the atoms by minimising the mismatch between these positions and their ideal positions. This is done in turn for each rigid structure and the maximum mismatch is kept track of for later use.

The fitting sequence works by calculating the rotational gradient of the mismatch of all the atoms within a rigid structure and then rotating the rigid structure by a small step down the gradient using equations 3.13 through 3.17,

$$\frac{\partial \epsilon^2}{\partial R_x^2} = 2\epsilon_x \frac{\partial \epsilon_x}{\partial R_x} + 2\epsilon_y \frac{\partial \epsilon_y}{\partial R_x} + 2\epsilon_y \frac{\partial \epsilon_z}{\partial R_x} \tag{3.13}$$

where $\frac{\partial \epsilon_x}{\partial R_x}$, $\frac{\partial \epsilon_y}{\partial R_x}$ and $\frac{\partial \epsilon_z}{\partial R_x}$ are given by,

$$\frac{\partial \epsilon_x}{\partial R_x} = V_y \left(\left(\frac{\frac{1}{4} R_x R_z}{\gamma} \right) + \frac{1}{2} R_y \right) + V_z \left(\left(\frac{-\frac{1}{4} R_x R_y}{\gamma} \right) + \frac{1}{2} R_z \right) \tag{3.14}$$

$$\frac{\partial \epsilon_y}{\partial R_x} = V_x \left(\left(-\frac{\frac{1}{4} R_x R_z}{\gamma} \right) + \frac{1}{2} R_y \right) - V_y R_x + V_z \left(-\gamma + \left(\frac{\frac{1}{4} R_x R_x}{\gamma} \right) \right) \tag{3.15}$$

$$\frac{\partial \epsilon_z}{\partial R_x} = V_x \left(\left(\frac{\frac{1}{4} R_x R_y}{\gamma} \right) + \frac{1}{2} R_z \right) + V_y \left(\gamma - \left(\frac{\frac{1}{4} R_x R_x}{\gamma} \right) \right) - V_z R_x \tag{3.16}$$

respectively and ϵ_x is given by,

$$\begin{aligned} \epsilon_x = \left(V_x \left(1 - \frac{1}{2} \left(R_y^2 + R_z^2 \right) \right) \right) + \left(V_y \left(-\gamma R_z + \frac{1}{2} \left(R_x R_y \right) \right) \right) \\ + \left(V_z \left(\gamma R_y + \frac{1}{2} \left(R_x R_z \right) \right) \right) - T_x \end{aligned} \tag{3.17}$$

In the above equations R_i is the i^{th} component of the "Rotor", a three dimensional vector which defines an axis about which to rotate and whose length gives the rotational angle in radians. V_i is the i^{th} component of the current position of a given atom in the rigid structure. T_i is the i^{th} component of the target position for said atom, in other words, where that atom has been moved to. Finally γ is $\sqrt{1 - \frac{1}{4}|R|}$.

The above equations can be permuted to generate the other components in the following way:

- $\frac{\partial \epsilon^2}{\partial R_x^2}$ can be changed by replacing the derivatives with their y and z counterparts.
- $\frac{\partial \epsilon_i}{\partial R_x}$ can be changed by permeating equations 3.14, 3.15 and 3.16 such that for ∂R_y the $\partial \epsilon_x$ term has the form of 3.16, $\partial \epsilon_y$ has the form of 3.14 and $\partial \epsilon_z$ has that of 3.15. Then within these equations all x, y and z terms must also be permeated such that all x's become z's and so forth.
- ϵ_x can be changed by permeating all the x, y and z terms such that all x's become z's as with the previous point.

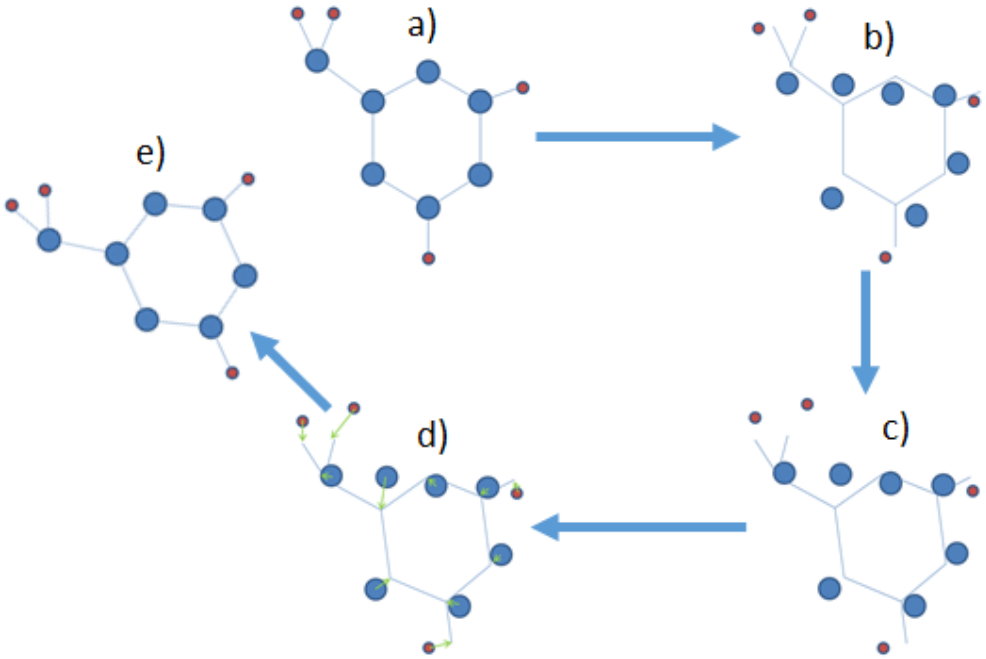

Figure 3.8: a) The atoms are displaced from the rigid structure. b) The rigid structure is rotated such to best fit the atoms with the smallest mismatch (in this image this is purely illustrative and may not be the minimum mismatch for the structure). c) The mismatch vectors are stored. d) Finally the mismatches are used to return the structure back to its ideally optimised form. e) shows the rotated version of the original body on which the algorithm can begin again.

.If the gradient is determined to be small enough then it can be assumed that the maximum mismatch is already less than the required tolerance and the fitting can be considered complete. If it is not then, after taking a step along the gradient, the gradient is recalculated. Once again, if this is small enough the fit is declared complete, if it is not then this gradient is compared to the previous one and if the difference is below a certain tolerance then it is safe to assume the body fitting is complete as the body is no longer moving between fitting attempts. An example diagram showing the process can be seen in figure 3.8

Once the fit is determined to be complete the mismatches between the ideal positions and their current positions are stored to be used later.

Next, steric collision detection is performed. All atoms are defined as being hard spheres that can have no steric overlap, as such the collision detection simply takes any atoms that are currently overlapping and works out a vector for each that points away from the collision overlap and is just large enough to bring them to the point of touching. These vectors are then stored for each atom also to be used later to relax the atoms.

Various values for the steric radii have been tested, however, those found in [74] were found to be the most practical for this type of simulation. It is also important to note at this point that atoms found within the same rigid structure cannot collide with each other. The reason for this is that due to the bonded environment being maintained by the rigid structure itself it is unnecessary to permit collisions between atoms within a structure, and in fact, if these were to be allowed many false collisions would be detected causing the optimised structure to be broken.

For complex molecules such as those studied in chapter 5 it was necessary to scale down the steric radii before performing simulations. The reason for this scaling down is due to the fact that dependent on the local environment an atom is in, its radius may deviate from its radius when in isolation. Due to this a large numbers of internal collisions were detected initially in some molecules, despite having been optimised with DFT. It was decided that the scaling would be uniform for all atoms within a molecule to ensure the overall shape of the molecule is not affected, and the scaling factor is determined by calculating the largest internal overlap between atoms in the molecule and shrinking these atoms down until they are only just in contact.

The collision detection efficiency was tested through various means. Ini-

tially a brute force all-atom collision check was used and was, of course, inefficient, however it did allow for the collision detection function to be tested. The first attempt to improve the efficiency was a regularly updated neighbour list, in which for a given number of fitting steps each atom maintained a list of all other possible atoms it could collide with in that time frame and only checked for collisions with those atoms. This improved the efficiency a lot, however, with larger system sizes the function to update the neighbour list became too inefficient to be practical. Finally a cell list was implemented and found to give the best improvement in efficiency, of around an order of magnitude faster.

With the rigid structure fitting and steric collision vectors generated for all atoms in the morphology the atoms can be relaxed. This is achieved by applying a move that is the sum of all of the stored vectors for each atom. Once this move has been made a check is performed to see whether the maximum mismatch and maximum collision vector is below a given tolerance. Typically these are a tenth of the defined movement step, and 0.1Å respectively. If these conditions are met the current fitting cycle is determined to be complete and the next cycle can begin, otherwise, the algorithm returns to the rigid structure fitting step and repeats this process until the exit condition is true.

As stated at the beginning of this section there are some optional parts to the algorithm that can be defined. The first is the option to reevaluate the moveset being used after a given number of steps. This is a useful option to have as it allows the moveset to adapt alongside the morphology. This in itself is quite a computationally expensive calculation however, so frequently updating the moveset can lead to much longer simulation times.

The second of the optional steps in the algorithm is to compress the

system. As stated in §3.1.1.a it is difficult to generate initial morphologies that are dense enough to perform charge transport calculations on. Therefore various compression techniques have been tested in order to take a randomly generated input and turn it into a useful starting point for our simulation needs.

The first method was a simple scaling of all coordinates in the system by a given percentage of the current system size. All atom coordinates were shrunk towards the origin, as was the cell size which periodic boundaries are applied over. The main problem with this is the amount of fitting cycles required to return the rigid structures to their optimised positions was large enough that it caused the total required simulation time to become too long (of the order of years). This clearly was not a suitable approach so some adaptations were made. Rather than applying a scaling to individual atoms in the system, scaling was applied to the centres of the rigid structures, such that all atoms in a rigid structure moved the same distance in the same direction. This reduced the number of fitting attempts required to fit the structures back to their atoms, however one problem still remained.

When the systems reached a higher density, performing a uniform scaling led to large amounts of tangling between atoms, and in some cases, structures like benzene rings interlocking. The first attempt to solve this was to a) reduce the size of the compression step and b) add an element of randomness to the scaling by not always moving everything directly towards the centre of the box, but choosing a vector that pointed towards that quadrant of space. This slightly alleviated the problem, however the randomness of the motion meant that on some occasions it made the problem worse. Thus this idea was scrapped and a different method used in its place. The new method was to allow the system to get to a point where tangling began to occur and then if a

large number of fitting attempts was required for one given cycle, temporarily switch the compression off. This gives the system a chance to relax into a state in which compression is then possible again. The temporary number of cycles compression is switched off for is defined to be a given number of cycles in which the number of fitting attempts is a small number, by default this was chosen to be less than ten cycles. This method proved to allow the systems to reach much higher densities successfully, and much faster than any previous attempts.

The final optional step is to take a snapshot of the current system state which writes out the atomic, rigid body centre and molecular coordinates along with a state file to allow the system to be reloaded at a later time. This is useful as for the compression part of a simulation it allows for sanity checks to be performed and ensure that the simulation is progressing correctly. It is also useful for fixed size simulations as the key to this technique of morphology generation is that it allows an exploration of conformational space. Thus taking many snapshots throughout the simulation gives a range of plausible morphologies upon which further analysis can be performed.

All of the points above highlight some of the hardest issues that were faced in adapting the FRODA algorithm to cope with multiple molecules rather than a single protein, with the key problems being generating sensible input morphologies without creating artefacts in the final results produced. The input generation alone required at least 6 months of work in order to prouduce morphologies which could be investigated. On top of this work into compression methods took a further 6 months. The addition of ellipsoids for both input generation and elastic modelling interactions was by far the largest challenge and throughout the last 18 months of the PhD was worked on and adapted in order to find an efficient and accurate method of determining the

intersection of the ellipsoids.

3.2 Charge Hopping Rates

Determining the rate at which charges can hop between molecules is essential for performing charge transport simulations. As discussed in §2.2 there are various methods of achieving this. For our purposes we have used Marcus rates as shown in [75] given by equation 2.1. With the exception of the transfer integral, these properties can be defined and approximated for the purposes of simulating organic semiconductors, with typical values of λ and ΔG^0 being of the order of 0.5eV. 0.5eV is used as it is typical of organic devices to work around these energy scales on the length scales in question, however, in future work these values will be calculated explicitly.

The transfer integral is determined by the overlap of the interacting electron orbitals and is also known as the effective coupling of two charge hopping sites. It is important to note that the transfer integrals for holes and electrons will be different, as they are dependent on the lowest unoccupied molecular orbital and highest occupied molecular orbital respectively, and therefore need to be calculated independently. The rest of this section will discuss the two possible routes employed in order to calculate these transfer integrals.

3.2.1 Quantum Chemistry Calculations

The first approach to calculating transfer integrals involves directly calculating electron orbitals and determining their overlap through density functional theory. As shown in figure 3.9 electron orbitals have complex shapes even for simple molecules. Thankfully there are software packages available that

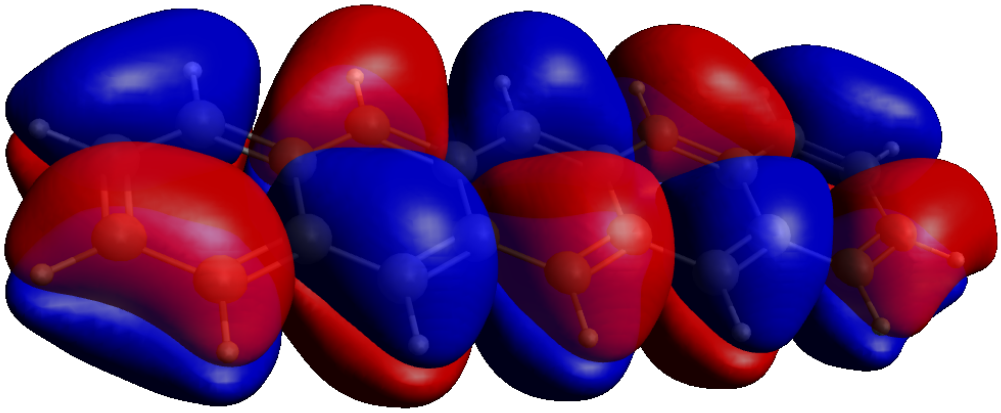

Figure 3.9: Example of the electron orbital shape of a pentacene molecule.

can calculate the properties of these orbitals and how they interact.

The QChem[76] software package was employed to calculate the effective coupling between molecules as it is capable of taking in two molecule fragments. The basic premise used to calculate the effective coupling involves calculating the orbitals for each individual fragment and then calculating the effects each of these fragment orbitals has on the other. Once this is achieved the coupling is determined by projecting one orbital onto the other and calculating the overlap.

In general these calculations are quite expensive to perform and, as such, approximations are necessary in order to make the use of these calculations practical. In this research, transfer integrals were calculated between pairs of molecules at set distances from the closest two molecules could be to each other and the cutoff distance determined as when the transfer integral has become negligible, and an exponential decay was fitted to the data such that we could interpolate values for the transfer integrals at any given distance.

3.2.2 VOTCA

An alternative method to the individual quantum chemistry calcualtions performed in the QChem package is VOTCA, a toolkit which allows for coupling to be calculated between all charge hopping sites in a morphology based on not only the distance but also the orientation of the sites [77]. This is beneficial due to the non-uniformity of electron orbital shapes. Firstly it takes an atomic morphology and separates it into conjugated segments as individual hopping sites. It then calculates the transfer integrals for all the interacting sites by means of the Zerners independent neglect of differential overlap (ZINDO) method[78], which as a semi-empirical method is faster than the full density functional theory calculations. It then goes on to calculate the reorganisation energies and site energy differences, thus generating all of the necessary components required to calculate Marcus rates.

3.3 Charge Transport Calculations

The final tool at our disposal for calculating the charge transport properties of materials is a kinetic Monte Carlo (KMC) method [79]. The premise of the model is to calculate the times for all possible events in the system to occur based on the calculated Marcus rates and a random element. The field is also used in order to bias the event times such that moving with the field is faster than moving against it. Once this event list has been created the events are executed based on the first reaction method, that is whichever event takes the shortest time to occur happens. The event times are then updated based on the time the previous event has taken and the effects that event has had on the system.

The initial setup of the KMC model requires a morphology, in the form of

a list of site coordinates (in nm) and types (cathode, anode or normal site). It also requires a neighbour list for each site in the system, containing a list of the site IDs along with the distances between them (also in nm). Finally it needs a specification of the energetics of the morphology consisting, for each site, of the highest occupied molecular orbital energy, the lowest unoccupied molecular orbital, the absorption coefficient (which is unnecessary for charge mobility calculations and is only important if illumination is used) and the transfer integrals for all neighbouring sites in eV.

The simulations are initially randomly seeded with electrons on a set number of sites, typically less than 10% of all sites in the system. The initial step of the simulation is to equilibrate for a certain amount of simulation time and then afterwards, to record data for the remaining duration of the simulation. The model supports multiple particle types, along with the choice of charge injection or illumination for photogeneration of current. The simulation also begins by seeding a set number of particles in the system. The simulations are periodic in two dimensions and the electrode contacts are at either end of the third. A bias can be applied between the electrodes and parameters such as the temperature can be defined. The mobilities calculated are found from an average of the mobility, in the direction of the field, of each charge in the system.

3.4 Summary

This chapter has focussed on the main body of work of the PhD, that is the development and adaptation of methods that allow for a robust method of calculating charge transport characteristics purely from atomic structure. The main contributions that have been made to the field would be the conver-

sion of single body FRODA to a multiple molecule input and the adaptation of the elastic modelling networks to use and elliposid based interaction volume. The software development side of all of this has been successful, albeit a very time consuming task. The combination of the morphology, charge hopping and charge transport methods is also something that has not generally been approached before and significant progress has been made towards creating a streamlined method of calculating the charge transport properties of molecules from their atomic structure. The simulation methods have also been designed to work on single core machines with runtimes typically less than 5 days from atomic structure to electron mobility.

Chapter 4

Validation of Morphology Techniques

This chapter investigates the validity of the methods used to generate morphologies discussed in chapter 3. Two molecules were chosen to be investigated, C60 as it is well represented by a sphere, and hexane due to it being a flexible chain. Input morphologies for these molecules were created using the random input generator, outlined in §3.1.1.a, at 4 different ellipsoid packing fractions ranging from 0.15 to 0.3. For each of the molecules, 5 input morphologies were generated for each of the 4 densities.

The C++ version of the FRODA code was used with a moveset generated at the initial step and used for the remainder of the simulations. The moveset used was the sum of the first 7 non-trivial eigenmodes calculated from the Hessian. The interaction volume for these calculations was taken to be twice that of the molecular minimum enclosing volume ellipsoid. C60 was treated as a single rigid body with a spherical interaction range, and hexane assumed to be comprised of 6 rigid bodies, each with its own interacting ellipsoid used in the Hessian moveset generation.

For these simulations the simulation dimensions were kept fixed (ranging from 100 Åto 150 Å) for the duration of the simulation so as to maintain the density and frames were recorded every 100 movement steps.

Figures 4.1 and 4.2 show the mean squared displacement measured for the geometric molecule centres throughout the course of the simulations. The mean squared displacement is calculated by summing the square of the distance each molecule has moved per cycle and then averaging by the number of molecules, and it is directly proportional to the diffusion coefficient. It can be seen that for each density that the diffusion coefficient is approximately constant and that this diffusion coefficient decreases as density increases. This makes sense as with lower densities there is more freedom for molecules to move around. It can also be seen from figure 4.3 that the diffusion coefficient of hexane molecules is lower than that of the C60 molecules. This is due to the fact that despite the hexane molecules being smaller and easier to push past each other, their flexibility allows them to tangle, possibly resulting in pairs of molecules getting stuck together. The spread in the mean squared displacements for systems of the same parameters is due to the random nature of the starting configurations leading to greater or fewer collisons.

Lennard-Jones potential energies, as defined in equation 4.1,

$$V(r) = 4\epsilon\left(\left(\frac{\sigma}{r}\right)^{12} - \left(\frac{\sigma}{r}\right)^{6}\right) \tag{4.1}$$

where ϵ is the minimum value, σ is the distance at which the potential is zero and r is the separation between geometric molecule centres, were summed for all interactions in each system throughout the simulations as they give a good indication of the energy state the system is currently in. It is important to note that FRODA does not evaluate energies, nor does it use

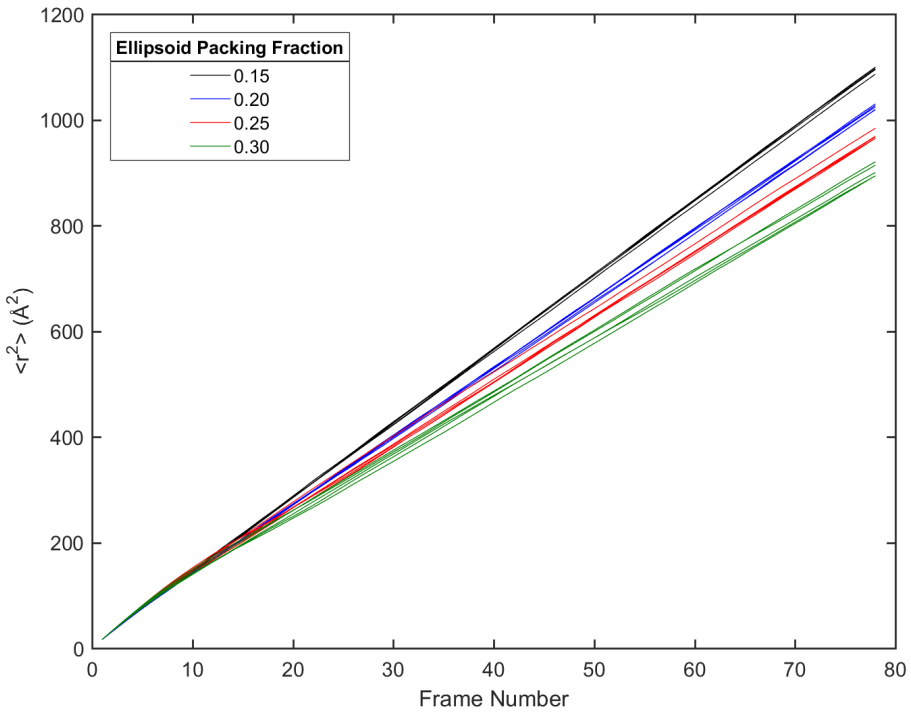

Figure 4.1: The mean squared displacements for geometric centres of molecules in morphologies of C60 generated from 5 simulation runs with different initial starting configurations.

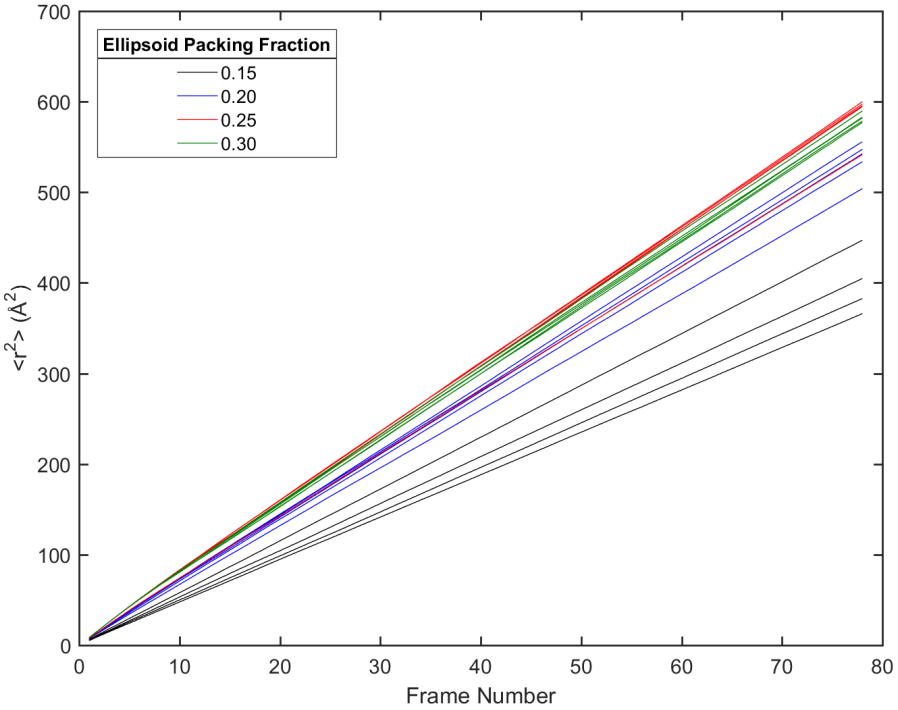

Figure 4.2: The mean squared displacements for geometric centres of molecules in morphologies of hexane generated from 5 simulation runs with different initial starting configurations.

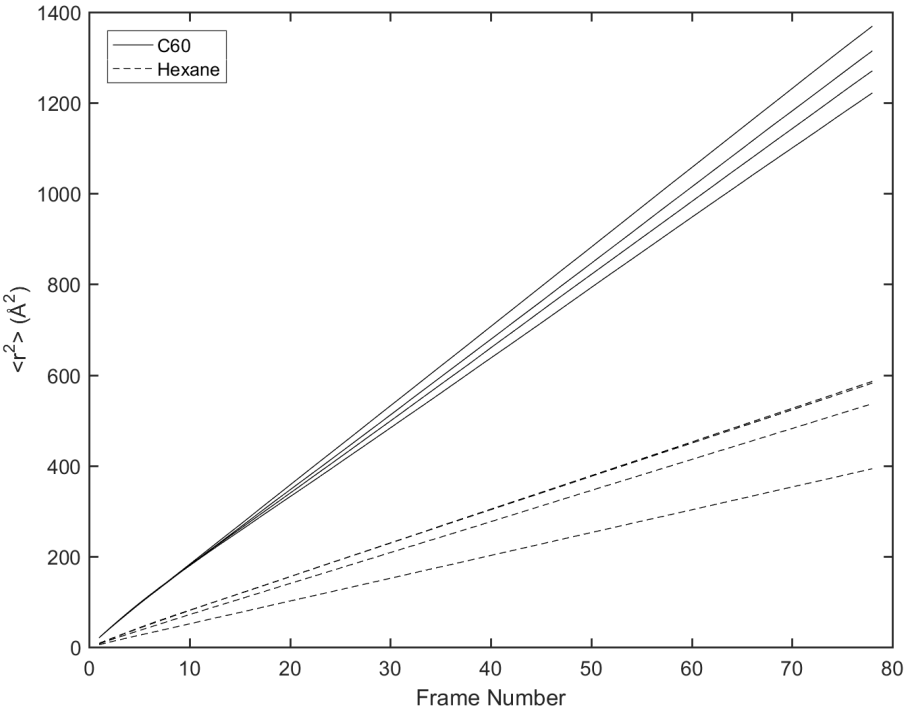

Figure 4.3: The averaged mean squared displacements for both C60 and hexane at varying densities.

them in any way to progress the simulation, however they are an interesting measure to make in post-processing to see what occurs throughout the simulations. Additionally as the energies are not used to direct the simulation and are purely for comparitive purposes, the constants ϵ and σ are set to unity. The results of this can be seen in figures 4.4 and 4.5 for C60 and hexane respectively. It can be seen that after a brief period of equilibration the energies tend to a relatively constant value. This is due to the fact that when the moveset is generated initially it is driving the molecules along a given set of phonon modes. By moving along these modes the energy should remain approximately constant as it is essentially equivalent to following a contour around the energy landscape. This is beneficial in that it allows us to know that for any given snapshot the energy of the system is constant and therefore comparing multiple snapshots is a reasonable approach to calculating properties of these morphologies. Hexane is less stable in energy than C60, this could be explained by the fact the hexane molecules are able to deform whereas the C60 molecules are completely rigid. It is also important to note that the hexane energies are two orders of magnitude greater, this is likely due to the tangling of molecules.

Radial distribution functions have been calculated to investigate the effect on structure based on density and also number of simulation steps elapsed. The radial distribution functions are calculated by counting the number of molecule centres in radial shells outward from each molecule centre in the system and comparing to the expected number of molecule centres if they were uniformly distributed throughout the system. This is performed for all molecules in the system and then averaged. In the case of the C60 morphologies, it can be seen in figure 4.6 that, except for the initial frame as it is before equilibriation, the radial distribution remains approximately the

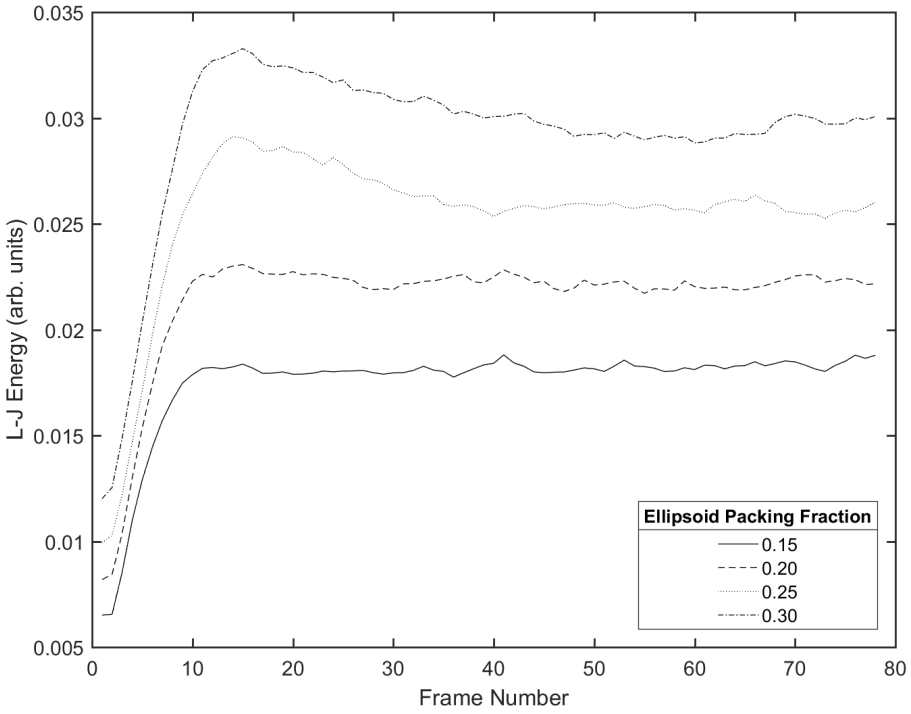

Figure 4.4: The average Lennard Jones potential energy measured throughout the morphology simulations for C60 at varying densities.

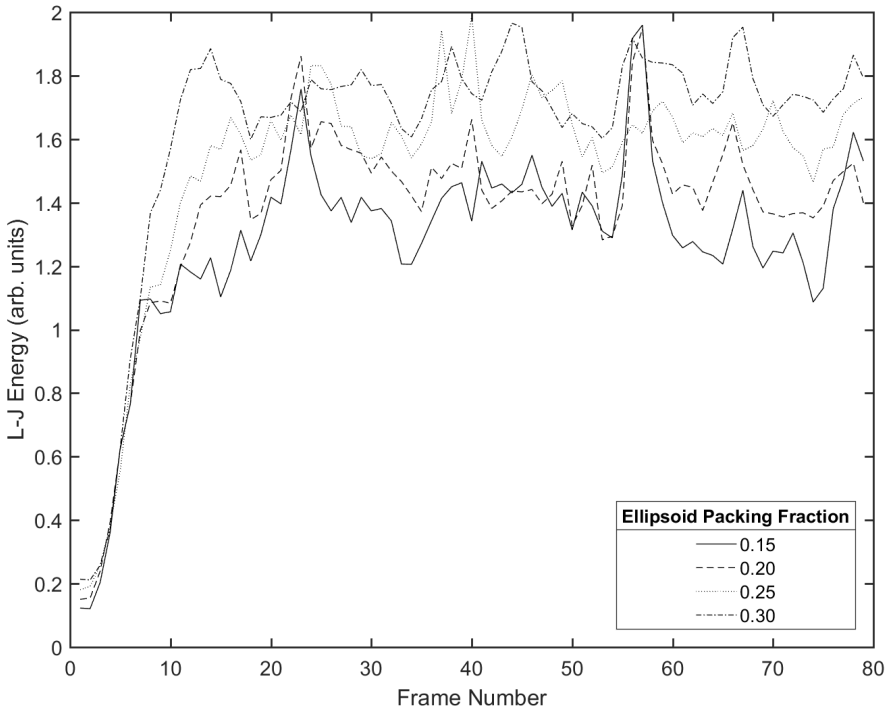

Figure 4.5: The average Lennard Jones potential energy measured throughout the morphology simulations for hexane at varying densities.

same. This is unsurprising as these simulations are analagous to hard sphere liquid simulations in which the radial distribution would remain unchanged. Density also appears to have little effect on the C60 morphologies' radial distribution functions, most likely due to the fact all of the densities used have enough free space such that the simulations should result in the same behaviour. This behaviour is shown in figure 4.8. An interesting point to note with the C60 morphologies is the strong peak at short distance but lack of second neighbour peak. This implies that the morphology is made up of clusters of nearest neighbours with voids between. Given the density of these morphologies this is not an unreasonable phenomena to see. The hexane morphologies radial distribution functions show slightly more variation with time, as seen in figure 4.7, and the initial region of the radial distribution appears to spread out over time. Once again, however, density seems to have little effect on these calculations as all distributions essentially overlap, as shown in figure 4.9. The variation in time makes some sense based on the previous arguments used for energy and mean squared deviation.

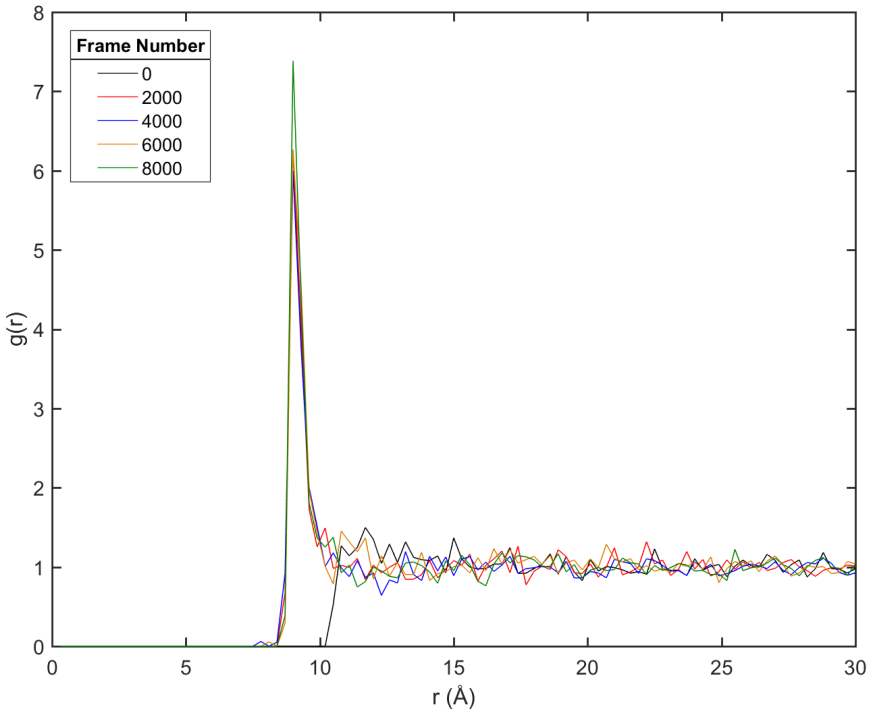

Figure 4.6: The radial distribution function for 5 frames of the morphology simulation of C60 at an ellipsoid packing fraction of 0.15. The initial frame does not show the nearest neighbour peak due to the initial random placement of molecules, however from frames 2000 onward this is shown.

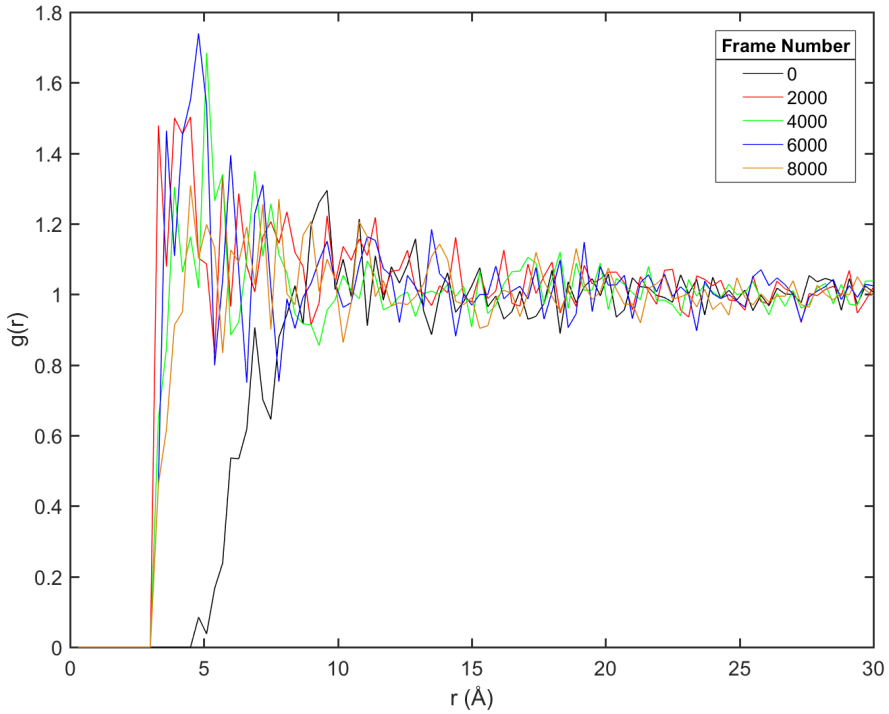

Figure 4.7: The radial distribution function for 5 frames of the morphology simulation of hexane at an ellipsoid packing fraction of 0.15.

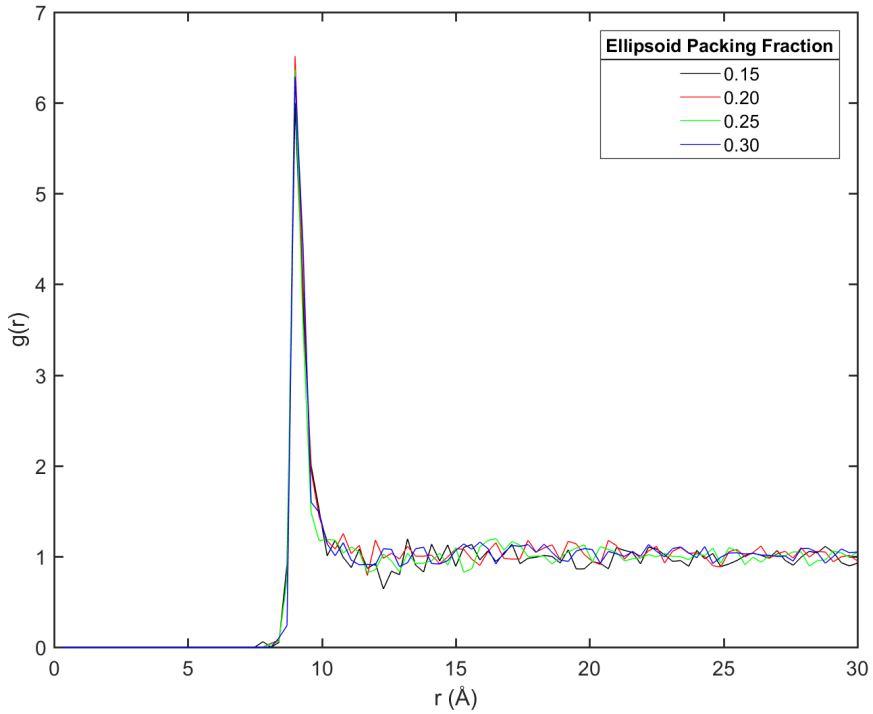

Figure 4.8: The radial distribution function at frame 4000 of the morphology simulation of C60 at varying densities.

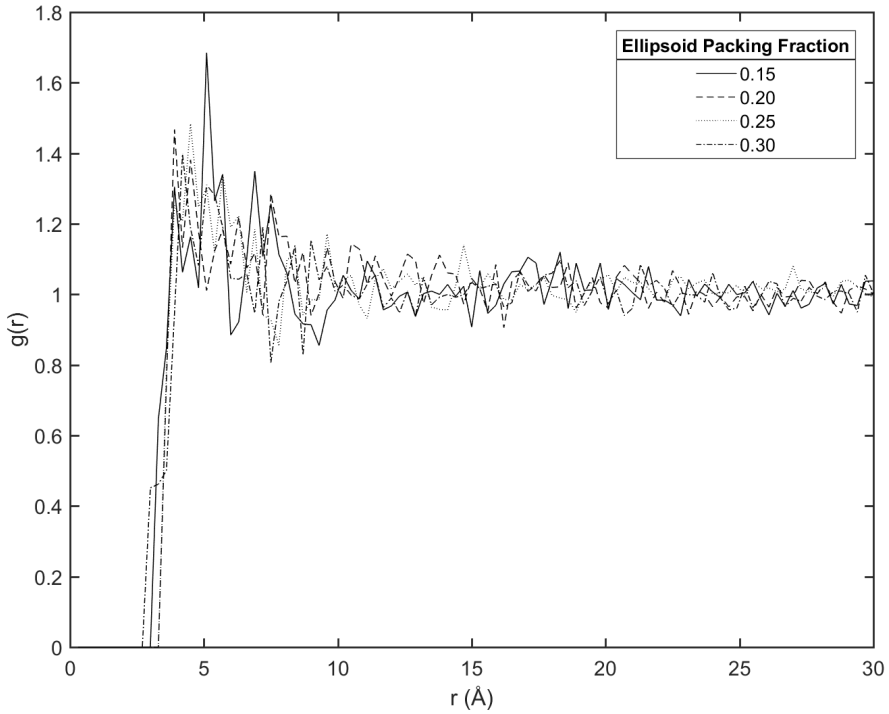

Figure 4.9: The radial distribution function at frame 4000 of the morphology simulation of hexane at varying densities.

Finally rotational correlation, $t(r)$, in which the angle between the smallest ellipsoid axes for two molecules is calculated, was measured for both C60 and hexane and a weighted distribution of angle against radial distance is shown in figures 4.10, 4.11, 4.12 and 4.13. The ellipsoid axes are predetermined on loading the molecules into the simulation and then rotated along with the molecules throughout the simulation, meaning the angles which are calculated are based on the updated ellipsoid axes. It comes as no surprise that the C60 morphologies exhibit no clear correlation in angle as they are spherical molecules so all orientations are equivalent. Hexane on the other hand shows correlation on the short range as seen by the peak at 4Å on frame 8000 in figure 4.11. This is probably due to the fact that, when collisions between these molecules occur, they are able to deform and essentially line up with each other.

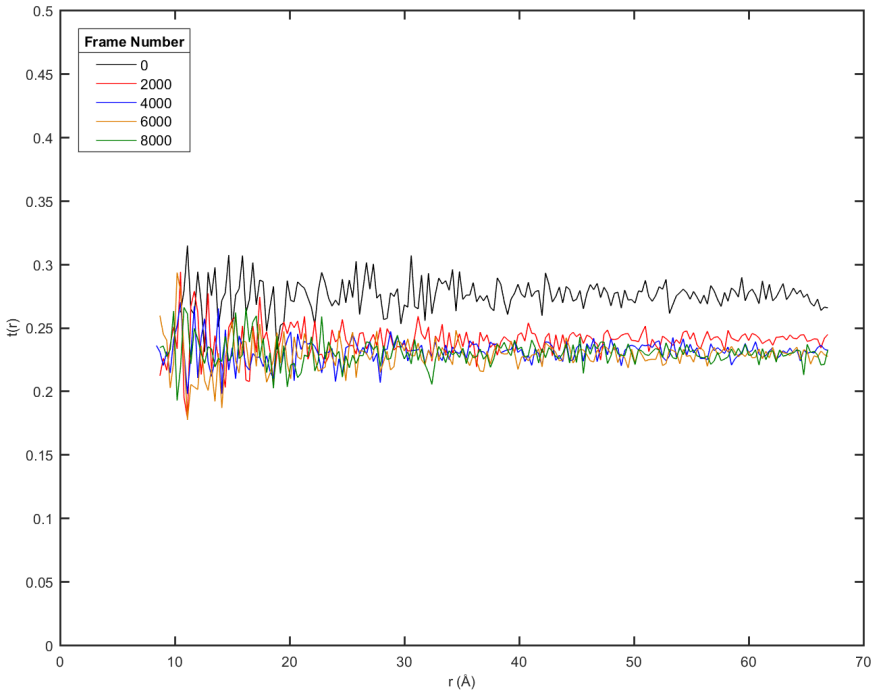

Figure 4.10: The orientational distribution function for 5 frames of the morphology simulation of C60 at an ellipsoid packing fraction of 0.15.

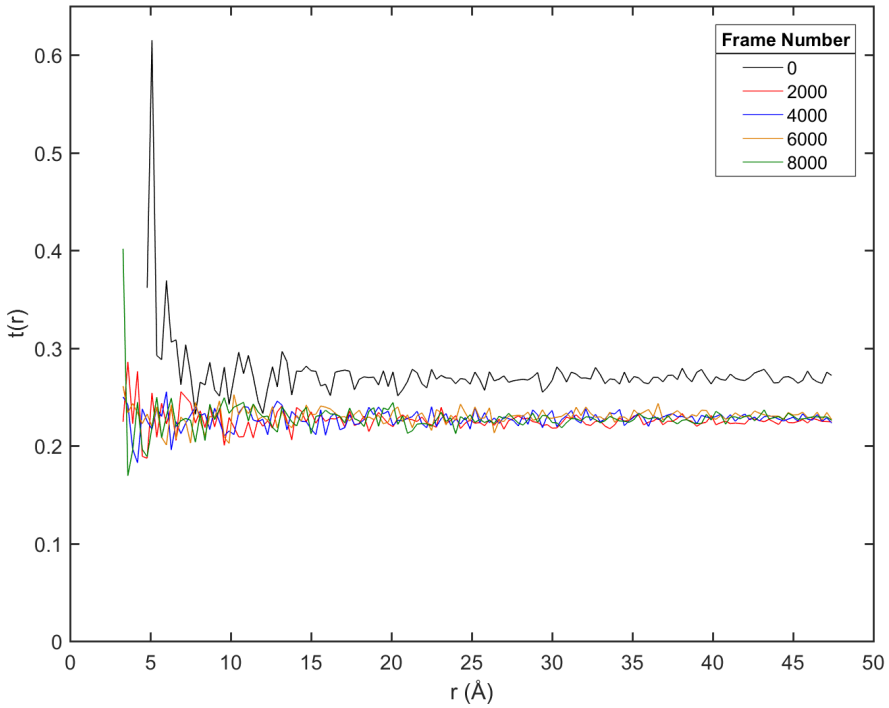

Figure 4.11: The orientational distribution function for 5 frames of the morphology simulation of hexane at an ellipsoid packing fraction of 0.15.

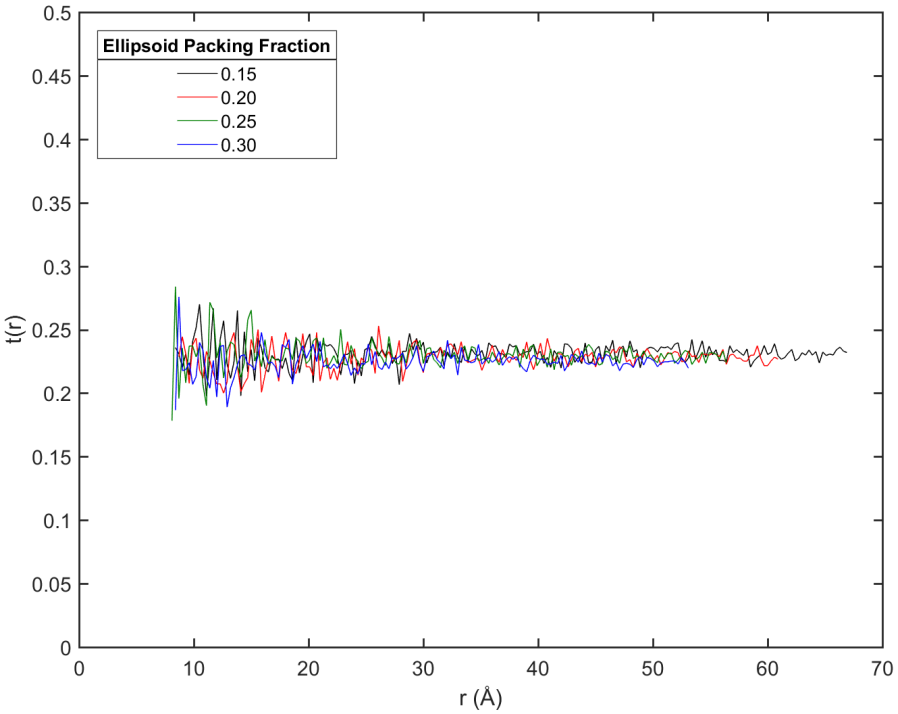

Figure 4.12: The orientational distribution function at frame 4000 of the morphology simulation of C60 at varying densities.

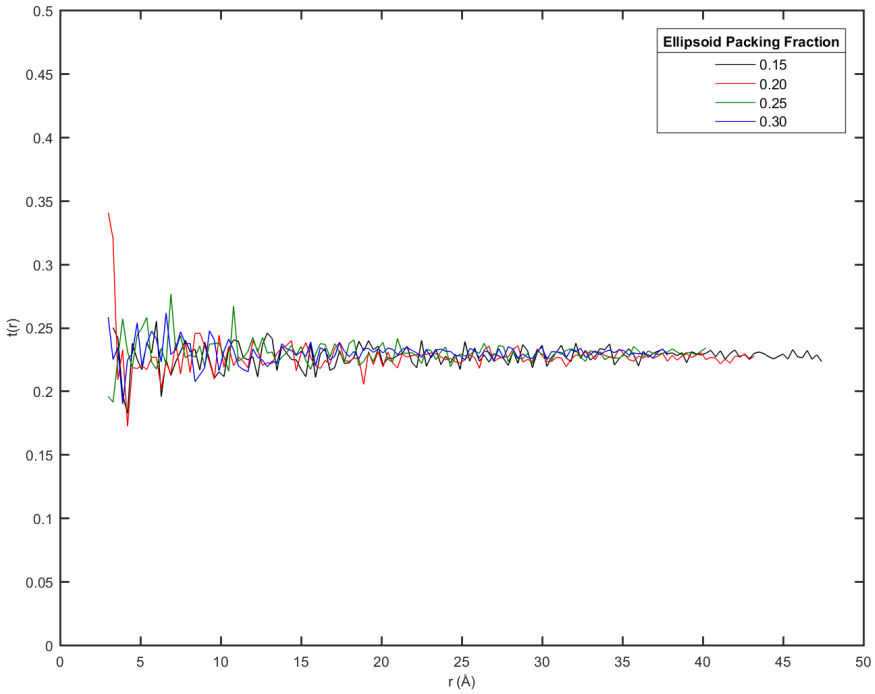

Figure 4.13: The orientational distribution function at frame 4000 of the morphology simulation of hexane at varying densities.

4.1 Conclusions

Overall the data shown throughout this chapter sets the foundation that the morphology methods used are not unreasonable, despite the approximations used. The morphologies exhibit the behaviour similar to that which would be expected based on the molecular structures used despite only being based on the rigidity of the molecule and steric interactions. The mean squared displacements are a good measure to support this statement as for the spherical C60 molecules exhibit more freedom to move than the flexible hexane chains that can interact with each other. The key results here also show the first time the FRODA methodology has ever been used to simulate small molecules and despite the limitations have shown promising results, especially since these results were generated on a single core in approximately 12 hours, which is around a fifth of the time equivalent molecular dynamics simulations would take. There are many additions that could be made to these methods, however, such as the inclusion of dipole interactions or inclusion of the rotational degrees of freedom in the Hessian moveset calculations, in order to better address the relative orientation of molecules.

Chapter 5

Investigating the Morphologies of Anthra[2,3-b:7,6-b']dithiophene Derivatives

This chapter will focus on analysis of the morphologies generated for a class of molecules known as anthra[2,3-b:7,6-b']dithiophene derivatives as they are of particular interest to our industry sponsor. This class of molecules consists of a dithiophene backbone with a series of sidechains linked by a triple carbon bond chain as shown in table 5.1.

The simulations were set up similar to the methods used in the previous chapter, with the main difference being that the initial morphologies were created as an ordered body-centred cubic-like structure at a density of 0.25g/cm^3 (which relates to box dimensions of approximately 200 by 200 by 125 Å). The rigid bodies for these molecules were created through the methods stated in section 3.1.1.a. Due to the deteministic nature of the

	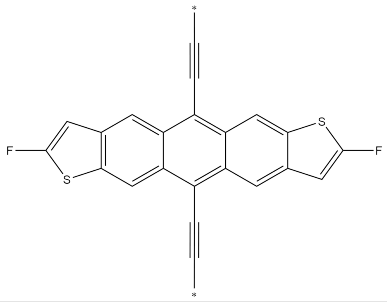				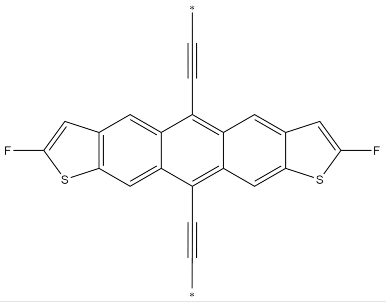
	A				B
1	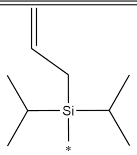	2	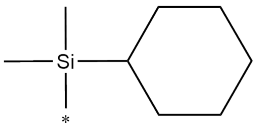	3	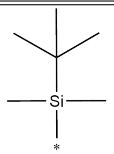
4	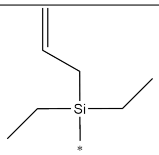	5	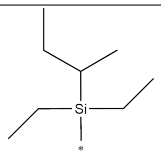	6	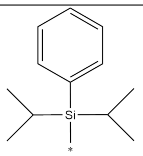
7	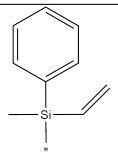	8	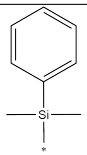	9	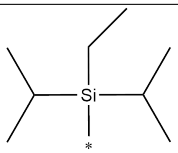
10	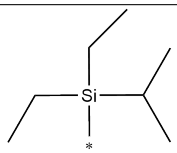	11	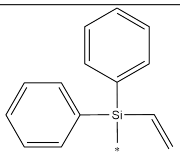	12	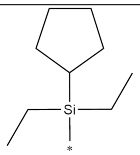
13	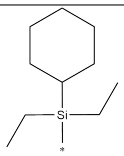	14	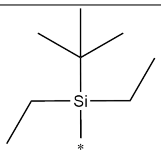	15	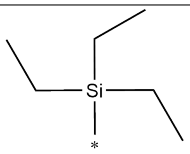

Table 5.1: The two isomers of the anthra[2,3-b:7,6-b']dithiophene backbones and the subsequent 15 sidechains investigated. The locations of the stars represent where the sidechains attach to the backbone.

simulation, in that the moveset generated at the beginning will be identical due to the ordered nature of the input, each morphology only required one simulation run to be performed.

Figures 5.1, 5.2 and 5.3 show the Lennard-Jones potential energies measured throughout the simulations for the 15 different molecules used. The energies remain relatively constant, although occasional peaks can be seen for some of the molecules. These occasional peaks could imply that those molecules have sidechains which induce structural order at close range and therefore, on occasion, the system exhibits higher energy when more collisions are occuring. Once molecules have managed to push past each other however the energy settles back to its typical value. Comparing the energies of all 15 molecules shows that they are all of a similar order and in general most of the molecules maintain a constant energy. This is useful as having similar energies implies the morphologies are in a similar state and therefore it is appropriate that the charge transport properties calculated for these morhologies can be compared.

The mean squared deviations for the molecules show quite a large range, as seen in figures 5.4, 5.5 and 5.6, with less bulky sidechains exhibiting a larger diffusion constant. This makes sense as these molecules would be more free to move around in the space available to them.

The radial distributions shown in figures 5.7-5.10 are much less well defined than those in the test cases shown in chapter 4. This is unsurprising as the molecules are much more complex in their strucure and have many flexible and rigid regions that can interact with each other. Certain sidechains exhibit similar behaviour in their radial distributions, an example of this is for side chains 2 and 8, shown in figures 5.7 and 5.8 respectively, where the initial peak in the distribution shifts to the left over the course of the simula-

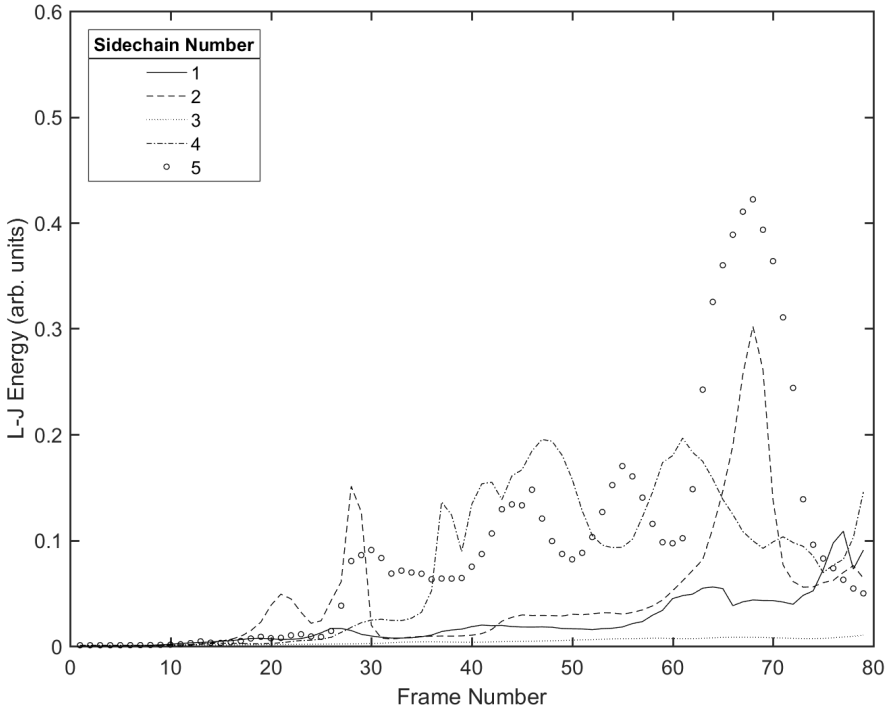

Figure 5.1: The Lennard-Jones potential energy calculated throughout morphology generation for molecules using sidechains 1 to 5.

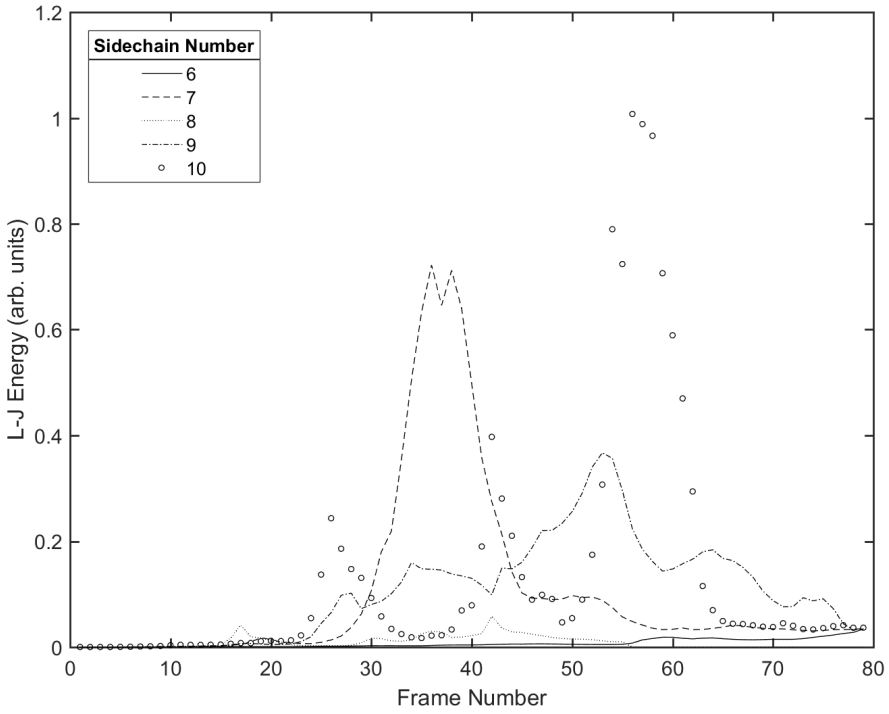

Figure 5.2: The Lennard-Jones potential energy calculated throughout morphology generation for molecules using sidechains 6 to 10.

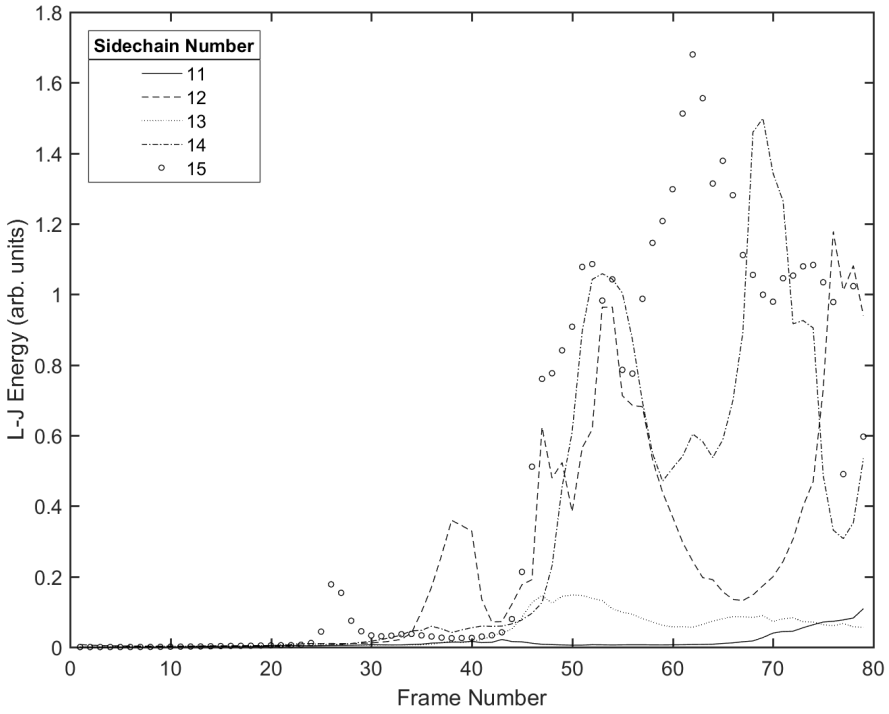

Figure 5.3: The Lennard-Jones potential energy calculated throughout morphology generation for molecules using sidechains 11 to 15.

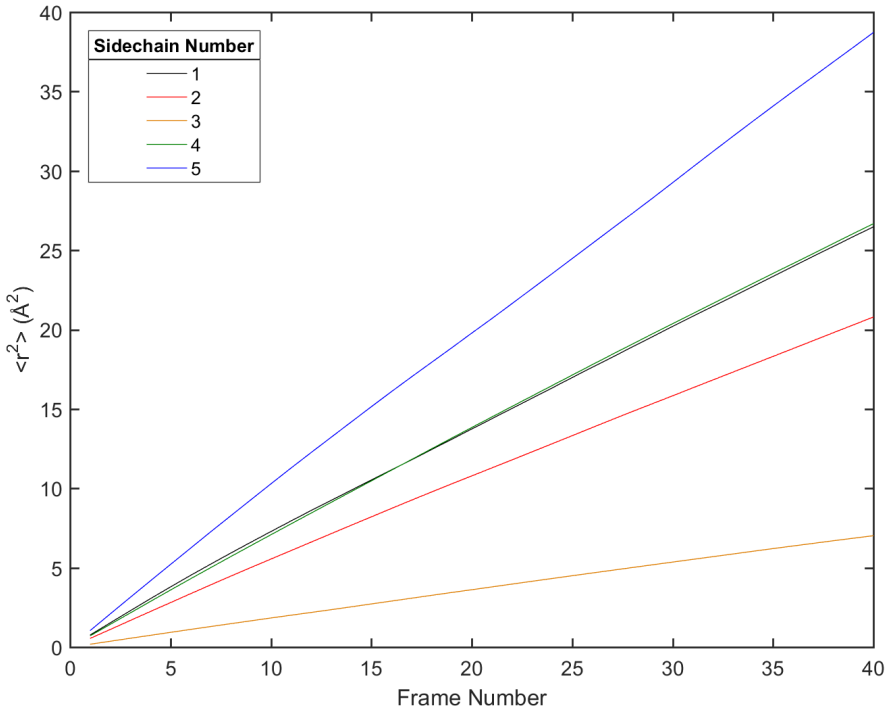

Figure 5.4: The mean squared displacement measured throughout morphology generation for molecules using sidechains 1 to 5.

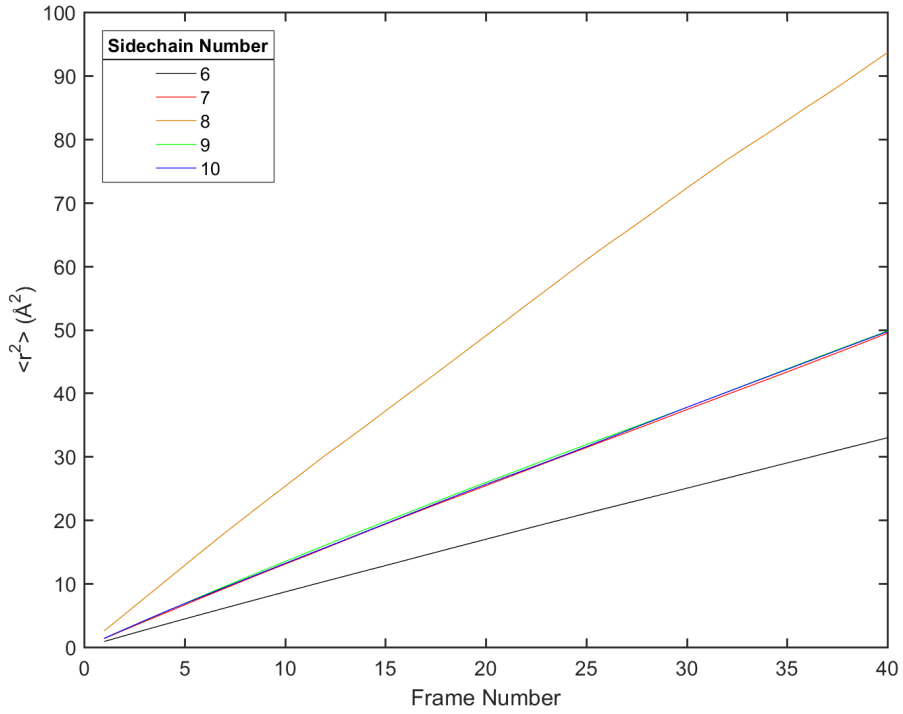

Figure 5.5: The mean squared displacement measured throughout morphology generation for molecules using sidechains 6 to 10.

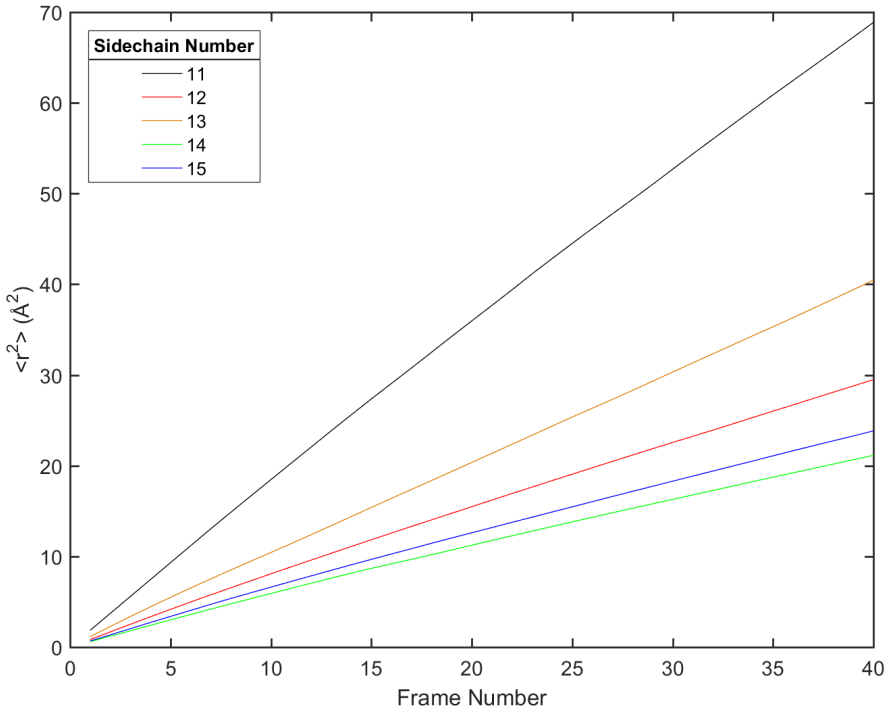

Figure 5.6: The mean squared displacement measured throughout morphology generation for molecules using sidechains 11 to 15.

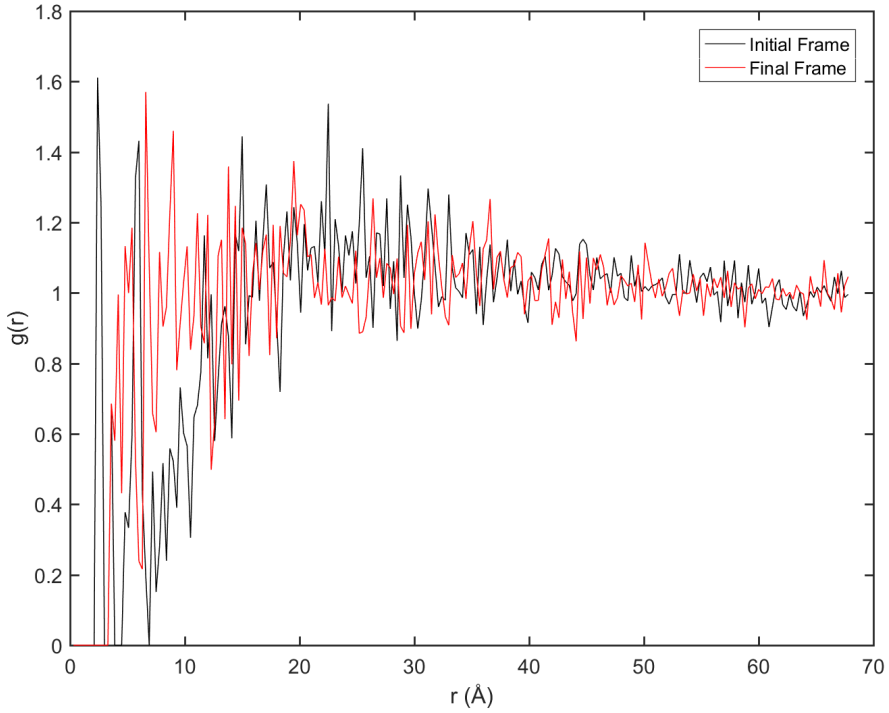

Figure 5.7: The radial distribution function calculated for an initial and final frame of the morphology generation for sidechain 2.

tion, whilst the distributions remain qualitatively similar. This trait can also be seen for sidechains 9 and 10, in figures 5.9 and 5.10 respectively. With reference to the molecular structures, 2 and 8, and, 9 and 10, do have similar properties, so it is not unreasonable to expect they should exhibit the same behaviour.

The rotational correlation functions, $t(r)$, can be seen for molecules 2, 8, 9 and 10 in figures 5.11-5.14. The trends seen in the radial distribution can also be seen here, however there are slight differences. The 2/8 pairing shows a decrease in correlation throughout the course of the simulation whereas the 9/10 pairing exhibits an increase in rotational correlation. The reason for this is the structures of the sidechains themselves. 9 and 10 could, when coming

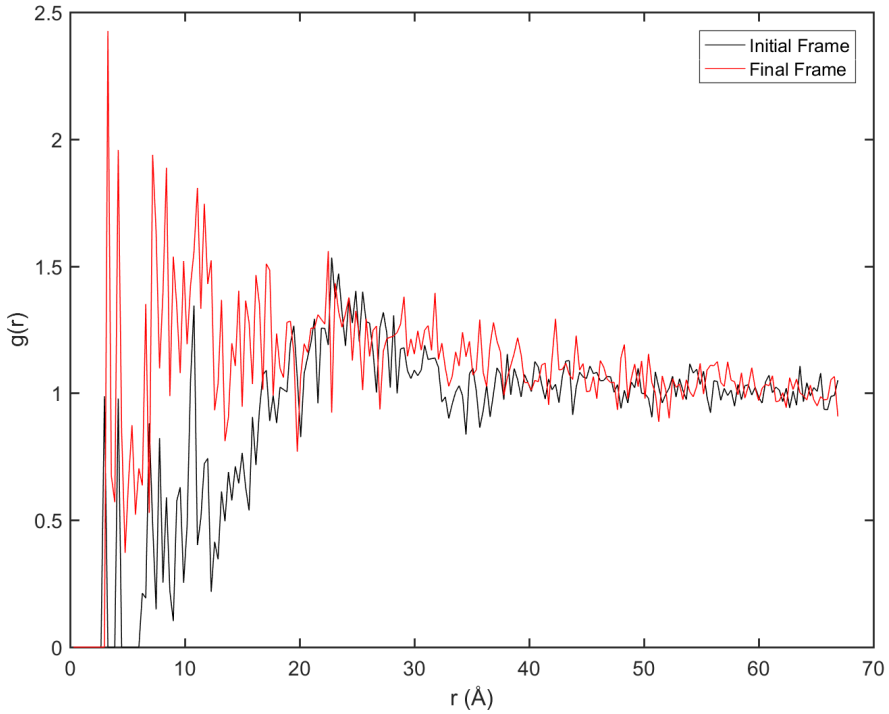

Figure 5.8: The radial distribution function calculated for an initial and final frame of the morphology generation for sidechain 8.

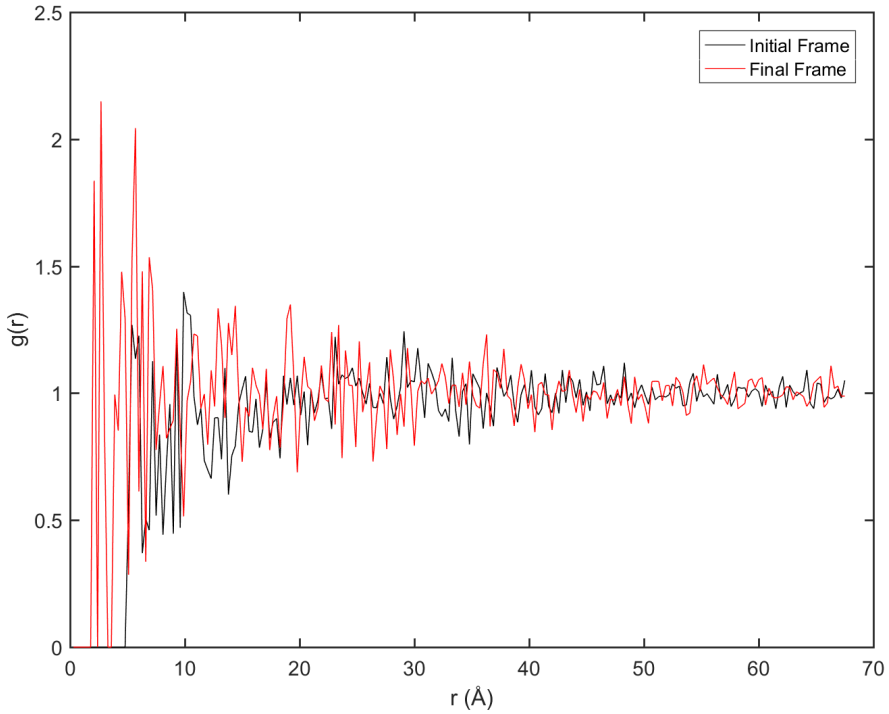

Figure 5.9: The radial distribution function calculated for an initial and final frame of the morphology generation for sidechain 9.

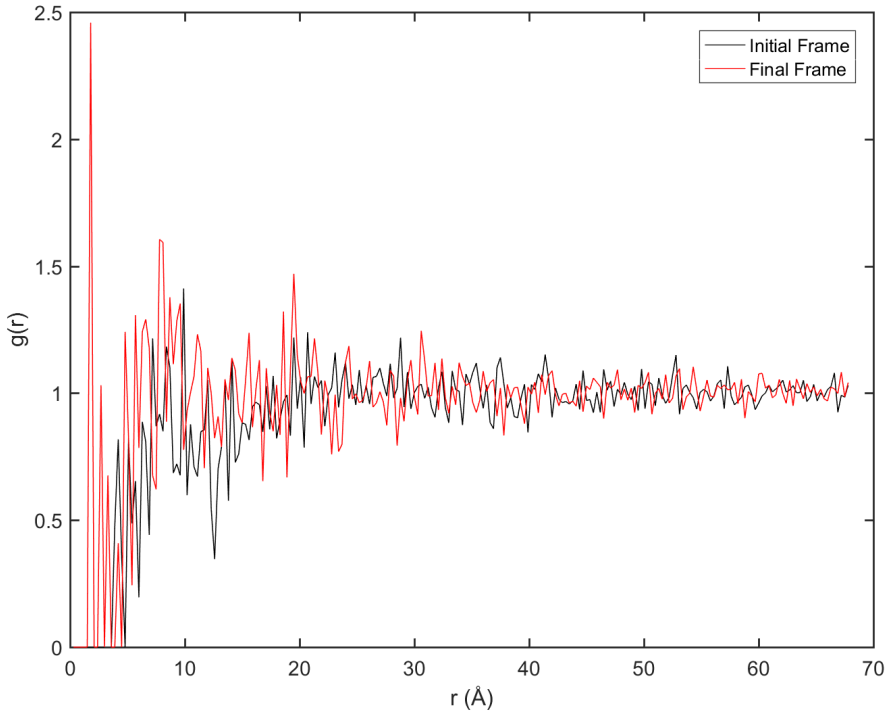

Figure 5.10: The radial distribution function calculated for an initial and final frame of the morphology generation for sidechain 10.

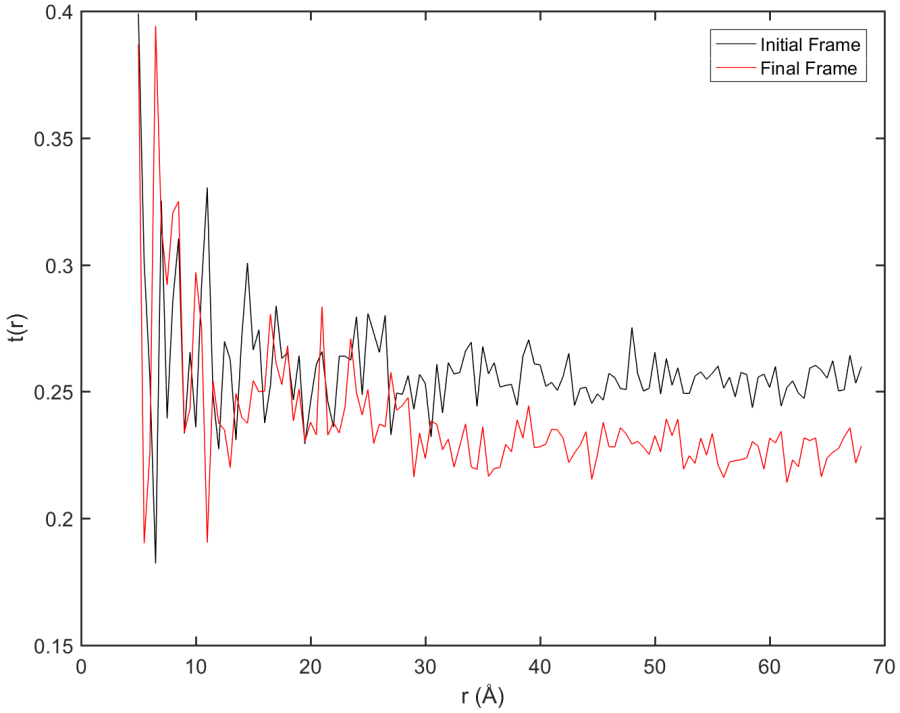

Figure 5.11: The orientational distribution function for an initial and final frame of the morphology generation for sidechain 2.

into close range, essentially become entangled causing alignment to occur between the molecules, whereas 2 and 8 have rigid bulky sections, which effectively would cause molecules to bounce away from each other rather than become attached. Overall the $t(r)$ distributions have a slightly higher baseline value as well suggesting some amount of long range correlation, this is most likely due to the umbrella like sidechains of the molecules limiting the movement of molecules once they are in close range forming ordered clusters.

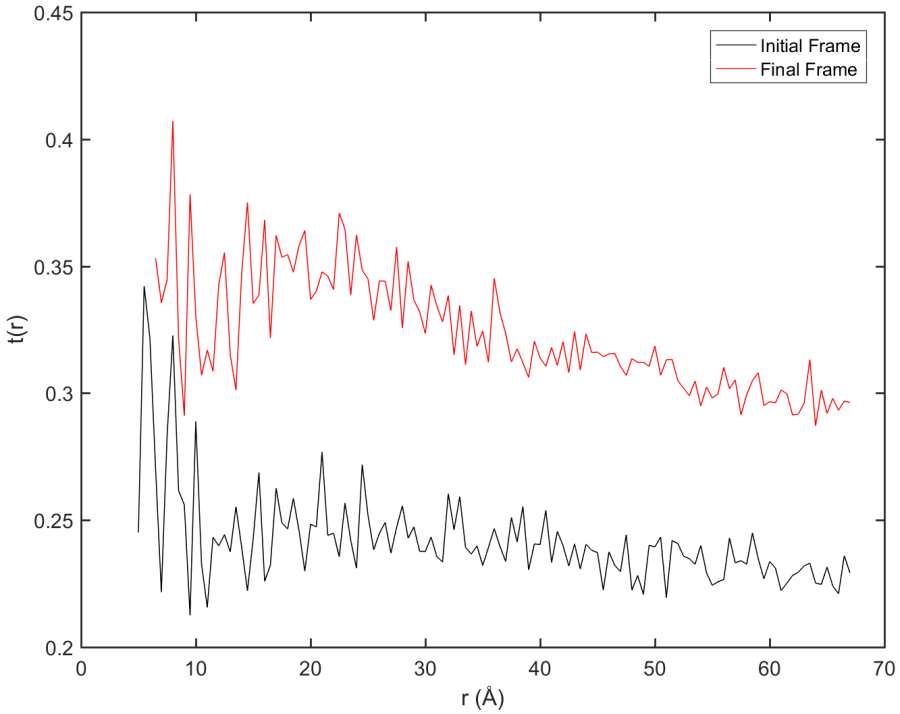

Figure 5.12: The orientational distribution function for an initial and final frame of the morphology generation for sidechain 8.

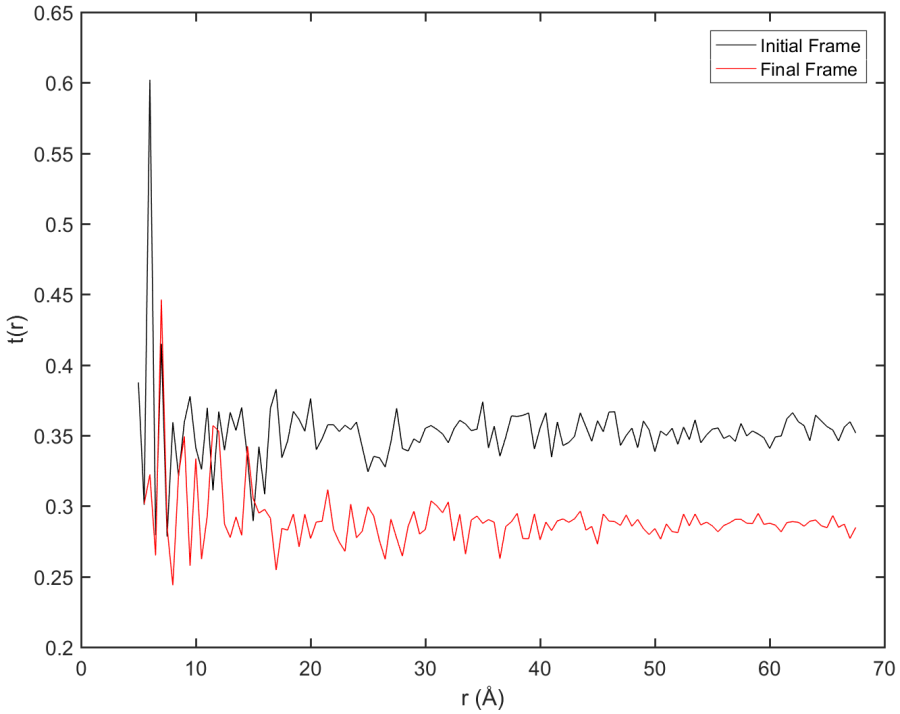

Figure 5.13: The orientational distribution function for an initial and final frame of the morphology generation for sidechain 9.

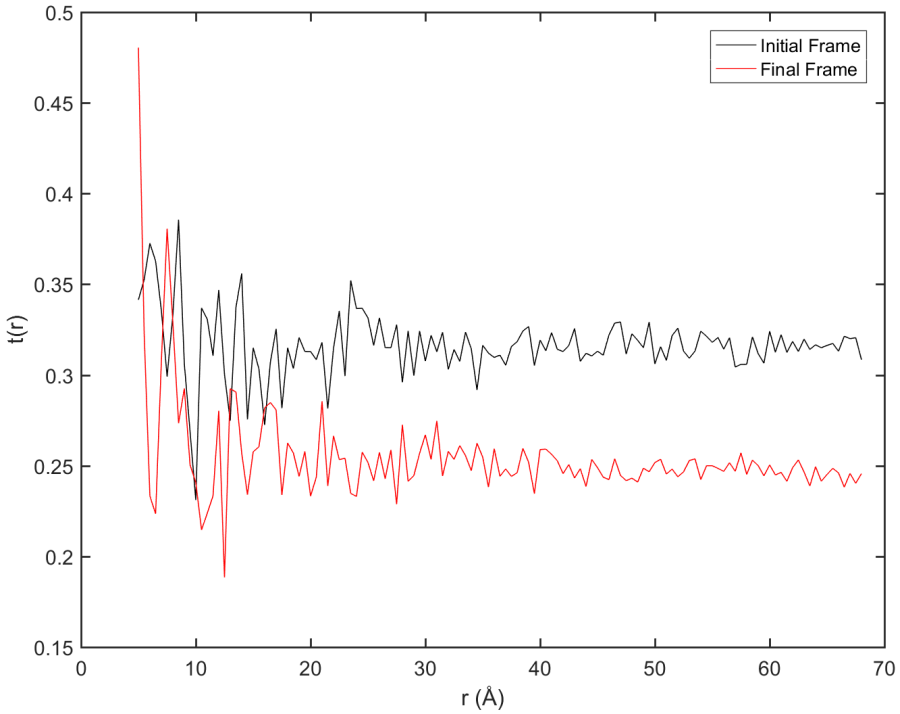

Figure 5.14: The orientational distribution function for an initial and final frame of the morphology generation for sidechain 10.

5.1 Conclusions

As a test case for this method, the similarities exhibited between the properties of the 15 morphological measurements made suggest that these morphologies will be appropriate for investigating the trends in charge transport for this class of molecules. There are clear indications of some level of short range order, however, overall the systems remain disordered, as is to be expected in amorphous organic semiconductors, and this allows for a suitable network of connected sites to be use for the kinetic Monte Carlo simulations.

Chapter 6

Charge Transport of Anthra[2,3-b:7,6-b']dithiophene Derivatives

This chapter focuses on the charge transport properties of the dithiophene derivative morphologies discussed in chapter 5.

Charge transport calculations were performed for three variations of the morphologies for the dithiophene derivatives using Ian Thompson's kinetic Monte Carlo code, the outline of which is shown in §3.3. Morphologies were either taken as being purely isomer A, purely isomer B or a blend containing 50:50 ratio of both isomers A and B. For each type of the 15 sidechains, 25 simulations were run and the mobilities averaged from the 25 runs. The 25 runs consisted of 5 simulations per morphology, of which there were 5 morphologies taken from the snapshots discussed in chapter 4. Due to the minor variation in structure between isomer A and isomer B it was decided that the morphologies of isomer A could also be used for isomer B, and then for the charge transport calculations these morphologies could be converted

by setting all sites to having the properties of either isomer A or B for the pure morphologies, and randomly assigning half of the sites as A or B for the 50:50 blend.

The simulations were set to equilibriate for 1 ns of simulation time and then measure for a further 3 ns allowing carriers to be able to travel the length of the cell. Initially 50 electrons were randomly seeded in the morphology of 716 sites, and a bias of 2 V applied across the electrodes. Electrons were chosen as the charge carrier despite holes being the primary carriers in dithiophenes. This was due to an issue with the use of holes in the kinetic Monte Carlo code not currently being supported. The reorganisation energy was taken to be 0.5 eV (for the reasons given in section §3.2), however in future work VOTCA will be used to calculate these energies explicitly. This is justified by the fact that the reorganisation energy is comprised of both an internal contribution, that is normally provided by quantum chemistry packages, and an external contribution from charges and dipoles involved in charge transfer that is, in itself, hard to estimate due to needing to be found for an entire film. Finally the simulations were run at a temperature of 300K.

The electron hopping rates were calculated using Marcus rates as discussed in §3.2 and the required transfer integrals were treated as an exponential decay with distance of the from shown in equation 6.1,

$$V = ae^{-kx} \tag{6.1}$$

with the coefficients determined using the QChem software package, shown in table 6.1. Each isomer backbone was treated as the hopping site and the effective coupling between an isomer A-isomer A pair, an isomer A-isomer B pair and an isomer B-isomer B pair was calculated for varying planar separation. A basis set of 6-21G (that is a basis set in which each core electron

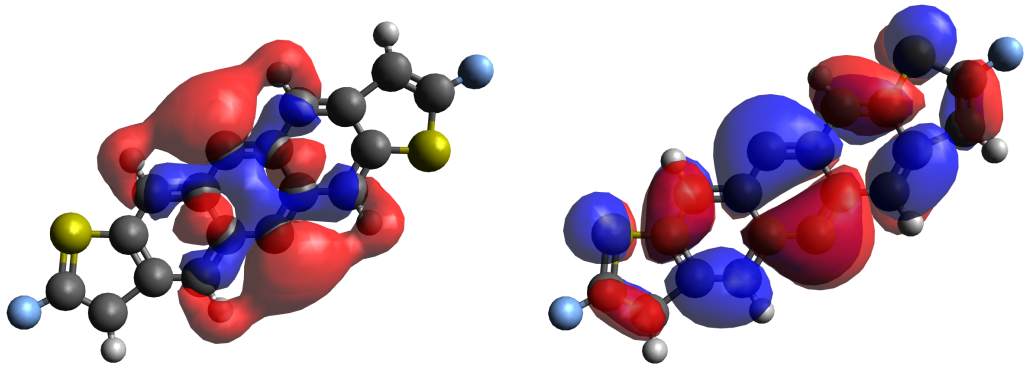

Figure 6.1: The lowest unoccupied molecular orbitals for isomer A (left) and isomer B (right) of the dithiophene backbones

	AA	AB	BA	BB
a	281.2	9.52	7.24	90.13
k	2.54	2.13	2.18	2.78

Table 6.1: Table of constants used for the exponential decays of transfer integrals of the dithiophene derivative isomers with distance calculated in equation 6.1. The columns indicate the constants used for electron transfer from isomer A to isomer A, isomer A to isomer B and so on.

orbital is defined by 6 primitive Gaussian functions, with the valence orbitals made up of two basis functions of 2 and 1 primitive Gaussian functions respectively) with a Hartree-Fock exchange (the method of determining the wavefunction through variational calculus) was used for all calculations as these are common methods used when investigating organics and are capable of dealing with the flourine atoms. Additionally the lowest unoccupied molecular orbital energy for each isomer was calculated in the same manner.

The mobilities calculated for the dithiophene derivatives are displayed in table 6.2. The errors shown were calculated as the standard error from the mean of the individual mobilities calculated from each simulation.

Initially, comparing the three columns of data, it is apparent that the

	Electron Mobility (cm^2 V^{-1} s^{-1})		
Sidechain \Isomer	AA	AB	BB
1	0.52 ± 0.10	0.09 ± 0.03	0.59 ± 0.08
2	1.34 ± 0.07	0.36 ± 0.07	1.37 ± 0.08
3	1.18 ± 0.04	0.26 ± 0.02	1.21 ± 0.10
4	1.92 ± 0.19	0.29 ± 0.05	1.21 ± 0.22
5	0.20 ± 0.04	0.05 ± 0.02	0.21 ± 0.05
6	0.50 ± 0.22	0.07 ± 0.03	0.57 ± 0.16
7	0.94 ± 0.10	0.21 ± 0.03	0.92 ± 0.17
8	1.16 ± 0.25	0.23 ± 0.13	1.21 ± 0.25
9	1.04 ± 0.22	0.18 ± 0.03	1.16 ± 0.20
10	0.81 ± 0.19	0.13 ± 0.01	0.84 ± 0.30
11	1.91 ± 0.69	0.31 ± 0.09	1.72 ± 0.24
12	1.56 ± 0.31	0.20 ± 0.04	1.65 ± 0.38
13	2.13 ± 0.19	0.36 ± 0.11	2.17 ± 0.27
14	0.31 ± 0.06	0.10 ± 0.03	0.41 ± 0.12
15	0.29 ± 0.04	0.10 ± 0.02	0.32 ± 0.03

Table 6.2: Electron mobilities, in the direction of applied field, calculated for the dithtiophene derivatives using a kinetic Monte Carlo simulation. The sidechain and isomer structures can be found in table 5.1 Columns AA, AB and BB refer to morphologies consisting of 100% isomer A, a 50:50 blend of isomers A and B and 100% isomer B respectively.

50:50 blend exhibits much lower mobilities than that of either of the pure morphologies. The reason for this is believed to be due to the lack of information on orientation in the transfer integral calcuations. This lack of orientation leads to much lower coefficients in the exponential terms for the AB transfer integral calculations. Figure 6.1 shows the lowest unoccupied molecular orbitals used for electron transfer in the simulation. It can be seen that when calculating purely a planar separation relation for the exponential decay of the transfer integrals for these isomers that, due to the difference in shape, a combination of the two isomers is likely to decay much faster than when one is interacting with another of the same type. It is also clear that there will be little difference in the exponential decays between the two self interacting isomers which is backed up by the data in table 6.2.

Focussing now on the pure columns of data, we see a clear variation in the mobilities based on the side chain which is used. It appears from the values seen that the more flexible arms a sidechain has the lower mobility it produces. This could be down to several reasons. However the most likely reason is that these sidechains can easily tangle causing molecules to become stuck a fixed distance apart from each other. Alternatively the sidechains with more rigid sections, such as benzene rings, will cause rotations between molecules when they collide which in turn causes an alignment of the conducting backbones (in this case represented by the centre of geometry) bringing them closer together. Exceptions to this rule are sidechains 1 and 6 which contain both a rigid benzene ring and two flexible carbon chains. In this situation the rigid area causes rotations which result in the other arms of the sidechain tangling which results in the same trend the purely flexible side chains exhibit. It is interesting to note that the relative sizes of the functional groups on the sidechains (see table 5.1) appear to only have a small impact on the

mobilities produced, however this further supports the argument that tangling and sterically induced rotation are the main causes for the difference in mobilities.

As these materials have not been investigated before we have no direct experimental data to compare with, however it is possible to compare to the literature on other dithiophene based molecules as they should exhibit fairly similar properties. In the literature it can be seen that most dithiophene molecules exhibit mobilities of the order 0.01 - 0.1 $cm^2V^{-1}s^{-1}$ [80] [81] [82]. This is an order of magnitude lower than what we see in our simulations, however this could be attributed to the high charge density in the systems and the lack of orientational information.

Much as it is possible to draw some conclusions from the mobilities shown in table 6.2 there are limitations to the methods currently used that may be affecting the results shown. The Marcus rates used for charge hopping rely on the reorganisation energy which has been approximated as described at the beginning of this chapter. As it currently stands, energetic disorder, which arises from polar groups within and between molecules interacting causing a change in site energy[83], has not been calculated for the morphologies used, meaning that the LUMO energies used are identical for all sites. The transfer integrals used are purely distance based and do not account for the orientation between charge hopping sites. These provide significant contributions to the charge hopping rates and thus in turn could be directly affecting the charge transport results produced. Additionally thermal activation has not been taken into account for long distance charge hopping due to the distance cutoff employed in the kinetic Monte Carlo method.

It is important to note however, that all simulations have been run under the same conditions and the only variation between simulations is that of the

molecular structure used therefore any approximations made should affect all the results in a similar manner. Additionally the trends seen in the mobilities appear to make sense from a structural point of view. That is not to say there is not more research to be done on these methods. Calculating transfer integrals for each individual pair of interacting molecules along with introducing energetic disorder into the morphologies would undoubtedly improve the accuracy of the calculated mobility estimates.

Chapter 7

Applications of Morphology Techniques to Organic Polymers

One of the main goals of this field of research is to eventually apply the FRODA methodology to investigating polymer-based organic semiconductors. Some preliminary work was completed on this matter, primarily looking at the difficulties around generating input structures, and how FRODA treats polymers in a similar way to how it treats proteins. The polymer of focus in this chapter is indacenodithiophene-benzothiadiazole (IDT-BT).

Initially, simulations were run on a single IDT-BT chain, that was produced by linearly attaching successive monomers together with the linking carbon bond distance calculated from DFT calculations on a dimer of IDT-BT. The result of this input generation can be seen in figure 7.1. After following the lowest energy mode the folded chain can be seen in figure 7.2. The flexing and torsional rotation between succesive monomers appears to qualitatively match well with that seen in published work [84]. It is im-

Figure 7.1: An initial input of a single IDT-BT polymer chain created as a linear chain of monomers.

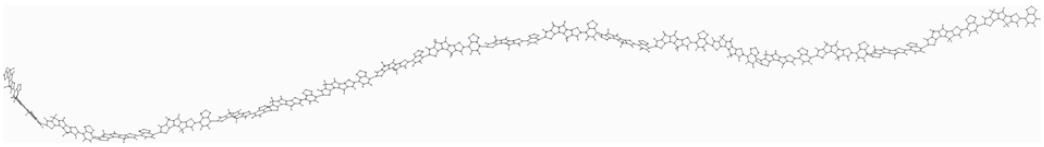

Figure 7.2: The final frame of the single chain IDT-BT simulation.

portant to note that these simulations were run on an older version of the FRODA code that used spherical interactions rather than those of ellipsoids. Additionally as polymers are known to retain some torsional order between successive monomers, tethers were implemented to ensure excessive torsional motion did not occur.

Figures 7.3 and 7.4 show the inital and end frames of a simulation of multiple IDT-BT chains. The initial input was created using the bounding box approach discussed in §3.1.1.a. Compression was also switched on in order to try and make the system reach the correct density. The primary problem with the polymer simulations is generating inputs at the correct density as to do so requires knowing how a chain is likely to fold to fit into a box. By generating a sparse input and compressing it we cannot know whether we are artificially affecting the way the chains fold and flex. This is apparent from the spiralling motion seen in the highlighted chain in figure 7.4.

Much as only preliminary work has been shown for the polymer chains in the course of this PhD, it is apparent that the techniques in FRODA are well suited to tackling the problem of generating polymer morphologies. The

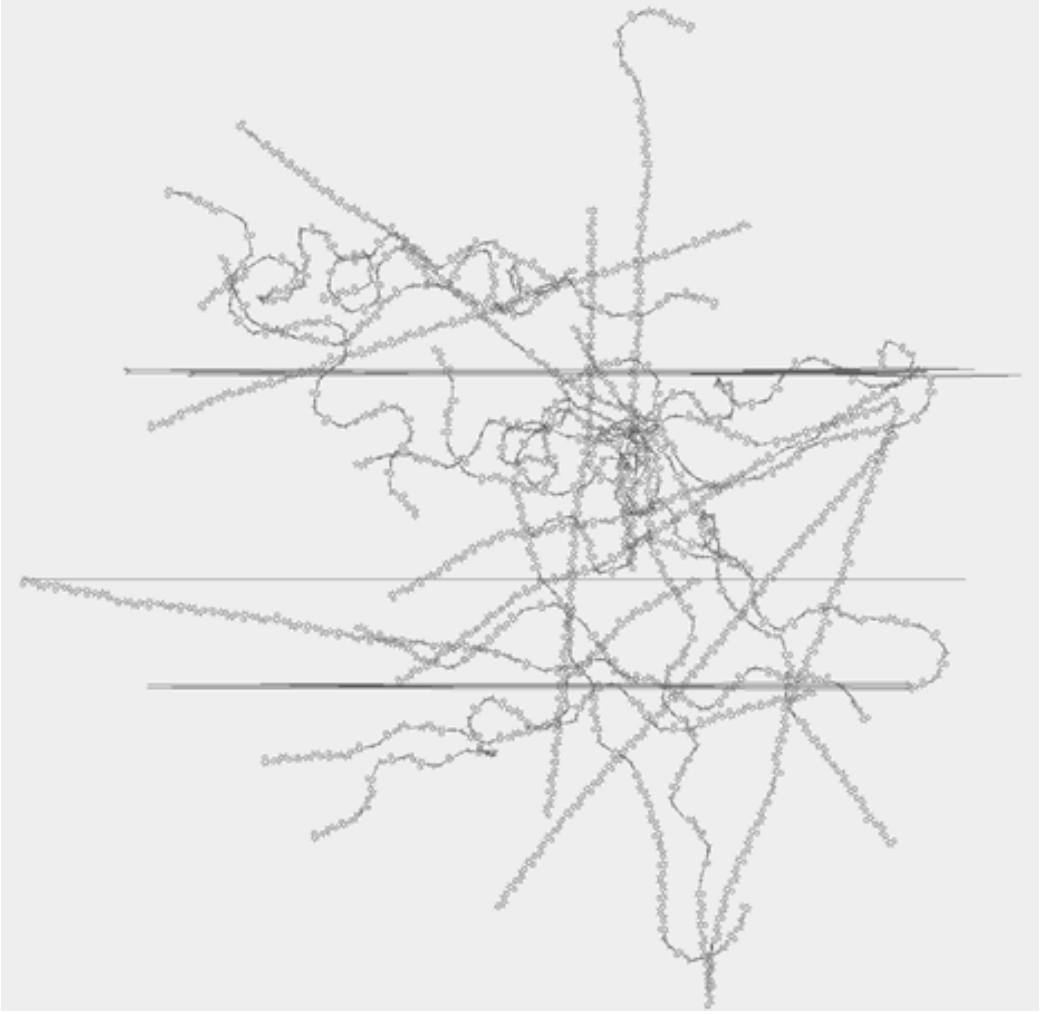

Figure 7.3: An initial input of randomly placed and oriented IDT-BT polymer chains of 20 monomers in length. The cell was a cube with dimensions of 12 nm.

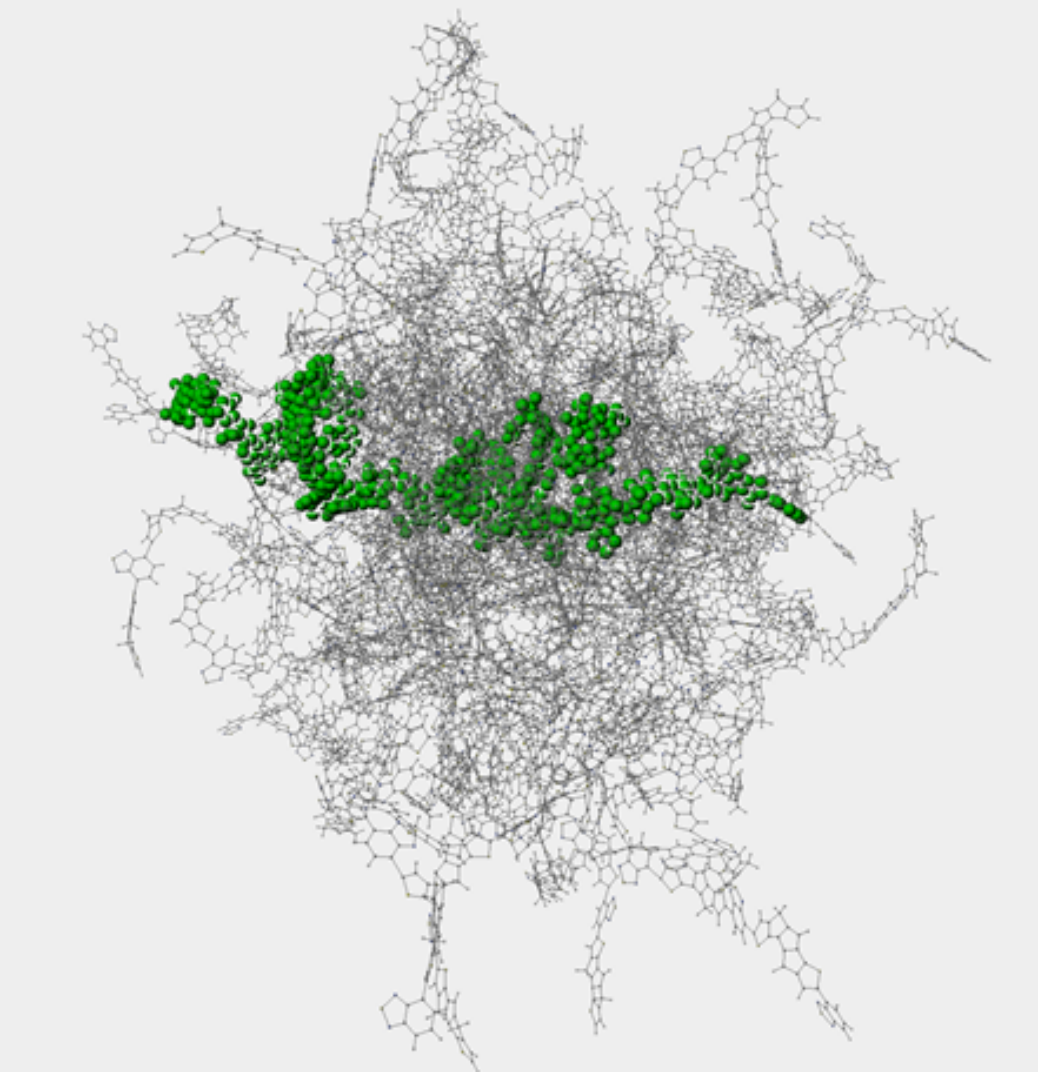

Figure 7.4: The final frame of the simulation performed on the input shown in figure 7.3. The cell size has been compressed such that the cube dimensions are approximately 6 nm.

main problem to overcome with this is the method of generating an input for polymers, however, taking outputs from other simulation techniques such as Monte Carlo methods may be a good place to start in solving this problem.

Chapter 8

Conclusions and Future Work

The overall aims of this project were to determine whether the FRODA methodology could be used to generate morphologies which were suitable for investigating the charge transport characteristics of materials based on their molecular structure, investigate methods for calculating hopping rates to be used in the charge transport calculations, and finally, to demonstrate that trends could be predicted for the electron mobilities of a set of molecules with similar structures.

Having reviewed the literature it is clear that this approach is a novel way of tackling the issue of charge transport in organic devices and the work on the project so far has shown clear promise for these methods being appropriate in calculating charge properties of materials from their atomic structures. The benefits to the methods are clear; the difference in time for these simulations to run is, in most cases, at least an order of magnitude faster than the current methods available. Additionally, having knowledge of the atomic configuration of morphologies without having to reverse engineer atomic locations (as in coarse grained models) allows for more accurate measurements of charge hopping characteristics to be performed.

The key work that was employed throughout the PhD was that of a methodological nature, rather than that of data collection. FRODA has been adapted to handle multiple molecules rather than single proton chains. This in itself is a great achievement and not an easy task to have completed. The addition of ellipsoids for interactions and input generation has improved the physical accuracy of the movesets generated, and removed the need for compression algorithms that can create artificial non-physical effects in the simulations. Above all else the ability to calculate mobilities from an atomic structure alone in typically less than 5 days is a vast improvement on the current available techniques.

The methods have been validated through using two key case study molecules, C60 and hexane. The morphology results shown in chapter 4 show that the morphologies produced are physically plausible and exhibit behaviours that would be expected based on molecular structure. The results also show the first ever data generated using FRODA on small molecules rather than large protein structures.

Having validated the methods, investigations into a class of dithiophene molecules have been performed, due to the interest of the industrial sponsor. These specific molecules have never been modelled before, and the charge transport data obtained from them shows trends that can be explained logically based on their structures.

A brief introduction to the work on polymers has also been shown, which is one of the avenues in which the future of this project lies. It has been shown for a single chain that FRODA is a good method to investigate the flexibility of polymers and with further work, it is planned that FRODA will eventually be able to generate large scale morphologies for polymer based organic semiconductors, a problem which is yet to be solved by other means.

There have been many successes with this work, however, that is not to say there is not more to do. With the morphology modelling, the addition of interactions such as dipoles and hydrogen bonding, could lead to more accurate descriptions of molecular morphologies to be studied. As for the charge hopping calculations, the implementation of VOTCA to calculate the various properties, such as reorganisation energy, transfer integrals and Gibbs free energies, can only lead to more accurate charge transport characteristics to be determined. Finally there are many more materials and devices that can be investigated, including device scale organic thin film transitsors or orphanic photovoltaic devices.

Appendix A

List of Software Versions Used

- Matlab - Version R2016b
- QChem - Version 4.3
- VMD - Version 1.9.3
- Gaussian09 - Version D.01
- ARPack++ - Downloaded from http://www.caam.rice.edu/software/ARPACK/download.html Feb 2017
- Mesh Kinetic Monte Carlo - Downloaded from https://gitlab.com/ABW_bath_group/Mesh_KMC_model April 2016
- GSL - Version 2.3

Bibliography

[1] D. M. Taylor. "Progress in organic integrated circuit manufacture". In: *Japanese Journal of Applied Physics* 55.2S (2015), 02BA01. DOI: 10.7567/jjap.55.02ba01.

[2] S.-B. Woo and J. H. Whealton. "Transport Model for Converting Charged Species in Drift Tubes". In: *Physical Review* 180.1 (1969), pp. 314–319. DOI: 10.1103/physrev.180.314.

[3] R. Munn and W. Siebrand. "Phono-limited transport of charge carriers in molecular crystals". In: *Chemical Physics Letters* 3.9 (1969), pp. 655–657. DOI: 10.1016/0009-2614(69)87001-6.

[4] B. J. Alder and T. E. Wainwright. "Phase Transition for a Hard Sphere System". In: *The Journal of Chemical Physics* 27.5 (1957), pp. 1208–1209. DOI: 10.1063/1.1743957.

[5] S. F. Edwards. "The statistical mechanics of polymers with excluded volume". In: *Proceedings of the Physical Society* 85.4 (1965), pp. 613–624. DOI: 10.1088/0370-1328/85/4/301.

[6] S. Gupta. "Computing aspects of molecular dynamics simulation". In: *Computer Physics Communications* 70.2 (1992), pp. 243–270. DOI: 10.1016/0010-4655(92)90191-z.

[7] J. Baschnagel et al. "On the construction of coarse-grained models for linear flexible polymer chains: Distribution functions for groups of consecutive monomers". In: *The Journal of Chemical Physics* 95.8 (1991), pp. 6014–6025. DOI: 10.1063/1.461826.

[8] L Muccioli et al. "Supramolecular Organization of Functional Organic Materials in the Bulk and at Organic/Organic Interfaces: A Modeling and Computer Simulation Approach". In: *Multiscale Modelling of Organic and Hybrid Photovoltaics*. Ed. by D. Beljonne and J. Cornil. Berlin, Heidelberg: Springer Berlin Heidelberg, 2014, pp. 39–101. ISBN: 978-3-662-43874-9. DOI: 10.1007/128_2013_470. URL: http://dx.doi.org/10.1007/128_2013_470.

[9] M. Ricci, R. Berardi, and C. Zannoni. "On the field-induced switching of molecular organization in a biaxial nematic cell and its relaxation". In: *The Journal of Chemical Physics* 143.8 (2015), p. 084705. DOI: 10.1063/1.4928522.

[10] M Lamarra et al. "Temperature dependence of charge mobility in model discotic liquid crystals". In: *Physical Chemistry Chemical Physics* 14.16 (2012), p. 5368. DOI: 10.1039/c2cp23178f.

[11] P. H. Verdier and W. H. Stockmayer. "Monte Carlo Calculations on the Dynamics of Polymers in Dilute Solution". In: *The Journal of Chemical Physics* 36.1 (1962), pp. 227–235. DOI: 10.1063/1.1732301.

[12] C. M. Guttman and E. A. DiMarzio. "Monte Carlo modeling of kinetics of polymer crystal growth: Regime III and its implications on chain morphology". In: *Journal of Applied Physics* 54.10 (1983), pp. 5541–5553. DOI: 10.1063/1.331835.

[13] J. Diani and P. Gilormini. "Molecular mobility with respect to accessible volume in Monte Carlo lattice model for polymers". In: *Physica A: Statistical Mechanics and its Applications* 468 (2017), pp. 825–831. DOI: 10.1016/j.physa.2016.11.088.

[14] D. J. Ashton, V. Sánchez-Gil, and N. B. Wilding. "Monte Carlo methods for estimating depletion potentials in highly size-asymmetrical hard sphere mixtures". In: *The Journal of Chemical Physics* 139.14 (2013), p. 144102. DOI: 10.1063/1.4824137.

[15] M. Mezei. "Estimation of the difference between molecular dynamics and monte carlo averages due to the truncation of the potential". In: *Chemical Physics Letters* 74.1 (1980), pp. 105–107. DOI: 10.1016/0009-2614(80)85024-x.

[16] B. R. Brooks et al. "CHARMM: The biomolecular simulation program". In: *Journal of Computational Chemistry* 30.10 (2009), pp. 1545–1614. DOI: 10.1002/jcc.21287.

[17] M. E. Tuckerman et al. "Efficient molecular dynamics and hybrid Monte Carlo algorithms for path integrals". In: *The Journal of Chemical Physics* 99.4 (1993), pp. 2796–2808. DOI: 10.1063/1.465188.

[18] J. D. Doll and H. K. McDowell. "Theoretical studies of surface diffusion: Self-diffusion in the fcc (111) system". In: *The Journal of Chemical Physics* 77.1 (1982), pp. 479–483. DOI: 10.1063/1.443630.

[19] J. D. Doll and D. L. Freeman. "A monte-carlo/molecular dynamics study of the diffusional recombination kinetics of C(a) +O(a) -¿ CO(g) on Pt(111)". In: *Surface Science* 134.3 (1983), pp. 769–776. DOI: 10.1016/0039-6028(83)90073-0.

[20] G. Bussi, D. Donadio, and M. Parrinello. "Canonical sampling through velocity rescaling". In: *The Journal of Chemical Physics* 126.1 (2007), p. 014101. DOI: 10.1063/1.2408420.

[21] S. Wells et al. "Constrained geometric simulation of diffusive motion in proteins". In: *Physical Biology* 2.4 (2005), S127–S136. DOI: 10.1088/1478-3975/2/4/s07.

[22] S. A. Wells, M. T. Dove, and M. G. Tucker. "Finding best-fit polyhedral rotations with geometric algebra". In: *Journal of Physics: Condensed Matter* 14.17 (2002), pp. 4567–4584. DOI: 10.1088/0953-8984/14/17/327.

[23] I. Bahar, A. R. Atilgan, and B. Erman. "Direct evaluation of thermal fluctuations in proteins using a single-parameter harmonic potential". In: *Folding and Design* 2.3 (1997), pp. 173–181. DOI: 10.1016/s1359-0278(97)00024-2.

[24] C. Chennubhotla et al. "Elastic network models for understanding biomolecular machinery: from enzymes to supramolecular assemblies". In: *Physical Biology* 2.4 (2005), S173–S180. DOI: 10.1088/1478-3975/2/4/s12.

[25] E. Eyal, L.-W. Yang, and I. Bahar. "Anisotropic network model: systematic evaluation and a new web interface". In: *Bioinformatics* 22.21 (2006), pp. 2619–2627. DOI: 10.1093/bioinformatics/btl448.

[26] S. A. Wells, J. E. Jimenez-Roldan, and R. A. Rmer. "Comparative analysis of rigidity across protein families". In: *Physical Biology* 6.4 (2009), p. 046005. DOI: 10.1088/1478-3975/6/4/046005.

[27] J. E. Jimenez-Roldan et al. "Integration of FIRST, FRODA and NMM in a coarse grained method to study Protein Disulphide Isomerase conformational change". In: *Journal of Physics: Conference Series* 286 (2011), p. 012002. DOI: 10.1088/1742-6596/286/1/012002.

[28] H. Li et al. "Protein flexibility is key to cisplatin crosslinking in calmodulin". In: *Protein Science* 21.9 (2012), pp. 1269–1279. DOI: 10.1002/pro.2111.

[29] S. A. Wells, S. J. Crennell, and M. J. Danson. "Structures of mesophilic and extremophilic citrate synthases reveal rigidity and flexibility for function". In: *Proteins: Structure, Function, and Bioinformatics* 82.10 (2014), pp. 2657–2670. DOI: 10.1002/prot.24630.

[30] S. A. Wells. "Geometric Simulation of Flexible Motion in Proteins". In: *Protein Dynamics*. Springer Nature, 2013, pp. 173–192. DOI: 10.1007/978-1-62703-658-0_10.

[31] S. A. Wells and A. Sartbaeva. "GASP: software for geometric simulations of flexibility in polyhedral and molecular framework structures". In: *Molecular Simulation* 41.16-17 (2015), pp. 1409–1421. DOI: 10.1080/08927022.2015.1032277.

[32] R. A. Römer et al. "The flexibility and dynamics of protein disulfide isomerase". In: *Proteins: Structure, Function, and Bioinformatics* 84.12 (2016), pp. 1776–1785. DOI: 10.1002/prot.25159.

[33] P. Doruker, A. R. Atilgan, and I. Bahar. "Dynamics of proteins predicted by molecular dynamics simulations and analytical approaches: Application to ?-amylase inhibitor". In: *Proteins: Structure, Function, and Genetics* 40.3 (2000), pp. 512–524. DOI: 10.1002/1097-0134(20000815)40:3<512::aid-prot180>3.0.co;2-m.

[34] A. Miller and E. Abrahams. "Impurity Conduction at Low Concentrations". In: *Physical Review* 120.3 (1960), pp. 745–755. DOI: 10.1103/physrev.120.745.

[35] J. Nelson et al. "Trap-limited recombination in dye-sensitized nanocrystalline metal oxide electrodes". In: *Physical Review B* 63.20 (2001). DOI: 10.1103/physrevb.63.205321.

[36] J. L. Bredas et al. "Organic semiconductors: A theoretical characterization of the basic parameters governing charge transport". In: *Proceedings of the National Academy of Sciences* 99.9 (2002), pp. 5804–5809. DOI: 10.1073/pnas.092143399.

[37] P. Hohenberg and W. Kohn. "Inhomogeneous Electron Gas". In: *Phys. Rev.* 136.3B (1964), pp. 864–871.

[38] W. Kohn and L. J. Sham. "Self-Consistent Equations Including Exchange and Correlation Effects". In: *Phys. Rev.* 140.4A (1965), pp. 1133–1138.

[39] A. K. Theophilou. "The energy density functional formalism for excited states". In: *Journal of Physics C: Solid State Physics* 12.24 (1979), p. 5419. URL: http://stacks.iop.org/0022-3719/12/i=24/a=013.

[40] S. M. Valone and J. F. Capitani. "Bound excited states in density-functional theory". In: *Phys. Rev. A* 23 (5 1981), pp. 2127–2133. DOI: 10.1103/PhysRevA.23.2127. URL: http://link.aps.org/doi/10.1103/PhysRevA.23.2127.

[41] J Katriel. "An alternative interpretation of Theophilou's extension of the Hohenberg-Kohn theorem to excited states". In: *Journal of Physics C: Solid State Physics* 13.15 (1980), p. L375. URL: http://stacks.iop.org/0022-3719/13/i=15/a=001.

[42] A. Görling. "Density-functional theory for excited states". In: *Phys. Rev. A* 54 (5 1996), pp. 3912–3915. DOI: 10.1103/PhysRevA.54.3912. URL: http://link.aps.org/doi/10.1103/PhysRevA.54.3912.

[43] Y. Sakiyama, S. Takagi, and Y. Matsumoto. "Validation of intermolecular pair potential model of SiH4: Molecular-dynamics simulation for saturated liquid density and thermal transport properties". In: *The Journal of Chemical Physics* 122.23 (2005), p. 234501. DOI: 10.1063/1.1931650.

[44] G. R. Hutchison, M. A. Ratner, and T. J. Marks. "Hopping Transport in Conductive Heterocyclic Oligomers: Reorganization Energies and Substituent Effects". In: *Journal of the American Chemical Society* 127.7 (2005), pp. 2339–2350. DOI: 10.1021/ja0461421.

[45] Y Li et al. "Theoretical Characterization of the PC60BM:PDDTT Model for an Organic Solar Cell". In: *The Journal of Physical Chemistry C* 115.44 (2011), pp. 21865–21873. DOI: 10.1021/jp2040696.

[46] P. Li et al. "External electric field-dependent photoinduced electron transfer of porphyrin–oligothiophene–fullerene triads". In: *Journal of Luminescence* 177 (2016), pp. 325–330. DOI: 10.1016/j.jlumin.2016.05.003.

[47] C Groves. "Simulating charge transport in organic semiconductors and devices: a review". In: *Reports on Progress in Physics* 80.2 (2016), p. 026502. DOI: 10.1088/1361-6633/80/2/026502.

[48] B. K. Crone et al. "Device model investigation of bilayer organic light emitting diodes". In: *Journal of Applied Physics* 87.4 (2000), pp. 1974–1982. DOI: 10.1063/1.372123.

[49] H. H. P. Gommans et al. "Field and temperature dependence of the photocurrent in polymer/fullerene bulk heterojunction solar cells". In: *Applied Physics Letters* 87.12 (2005), p. 122104. DOI: 10.1063/1.2056609.

[50] G. A. H. Wetzelaer et al. "Trap-assisted and Langevin-type recombination in organic light-emitting diodes". In: *Physical Review B* 83.16 (2011). DOI: 10.1103/physrevb.83.165204.

[51] M. Koehler, I. Biaggio, and M. G. E. da Luz. "Resolving the contact voltage dilemma in organic field effect transistors". In: *Physical Review B* 78.15 (2008). DOI: 10.1103/physrevb.78.153312.

[52] J. A. Barker, C. M. Ramsdale, and N. C. Greenham. "Modeling the current-voltage characteristics of bilayer polymer photovoltaic devices". In: *Physical Review B* 67.7 (2003). DOI: 10.1103/physrevb.67.075205.

[53] L. J. A. Koster et al. "Device model for the operation of polymer/fullerene bulk heterojunction solar cells". In: *Physical Review B* 72.8 (2005). DOI: 10.1103/physrevb.72.085205.

[54] A. Massé, R. Coehoorn, and P. Bobbert. "Universal Size-Dependent Conductance Fluctuations in Disordered Organic Semiconductors". In: *Physical Review Letters* 113.11 (2014). DOI: 10.1103/physrevlett.113.116604.

[55] B. P. Lyons, N. Clarke, and C. Groves. "The Quantitative Effect of Surface Wetting Layers on the Performance of Organic Bulk Heterojunction Photovoltaic Devices". In: *The Journal of Physical Chemistry C* 115.45 (2011), pp. 22572–22577. DOI: 10.1021/jp2078709.

[56] Z. G. Yu et al. "Molecular Geometry Fluctuation Model for the Mobility of Conjugated Polymers". In: *Physical Review Letters* 84.4 (2000), pp. 721–724. DOI: 10.1103/physrevlett.84.721.

[57] M. Casalegno, A. Bernardi, and G. Raos. "Numerical simulation of photocurrent generation in bilayer organic solar cells: Comparison of master equation and kinetic Monte Carlo approaches". In: *The Journal of Chemical Physics* 139.2 (2013), p. 024706. DOI: 10.1063/1.4812826.

[58] J. Zhou et al. "Carrier density dependence of mobility in organic solids: A Monte Carlo simulation". In: *Physical Review B* 75.15 (2007). DOI: 10.1103/physrevb.75.153201.

[59] H. Houili et al. "Investigation of the charge transport through disordered organic molecular heterojunctions". In: *Journal of Applied Physics* 100.3 (2006), p. 033702. DOI: 10.1063/1.2222041.

[60] S. L. M. van Mensfoort and R. Coehoorn. "Effect of Gaussian disorder on the voltage dependence of the current density in sandwich-type devices based on organic semiconductors". In: *Physical Review B* 78.8 (2008). DOI: 10.1103/physrevb.78.085207.

[61] M. Casalegno et al. "Coarse-grained kinetic modelling of bilayer heterojunction organic solar cells". In: *Organic Electronics* 13.5 (2012), pp. 750–761. DOI: 10.1016/j.orgel.2012.01.024.

[62] S. E. J. O'Kane et al. "Measurement and modelling of dark current decay transients in perovskite solar cells". In: *J. Mater. Chem. C* 5.2 (2017), pp. 452–462. DOI: 10.1039/c6tc04964h.

[63] K. Feron et al. "Utilizing Energy Transfer in Binary and Ternary Bulk Heterojunction Organic Solar Cells". In: *ACS Applied Materials & Interfaces* 8.32 (2016), pp. 20928–20937. DOI: 10.1021/acsami.6b05474.

[64] H. Bssler. "Charge Transport in Disordered Organic Photoconductors a Monte Carlo Simulation Study". In: *physica status solidi (b)* 175.1 (1993), pp. 15–56. DOI: 10.1002/pssb.2221750102.

[65] H. Li et al. "Relationship between Mobilities from Time-of-Flight and Dark-Injection Space-Charge-Limited Current Measurements for Organic Semiconductors: A Monte Carlo Study". In: *The Journal of Physical Chemistry C* 118.12 (2014), pp. 6052–6058. DOI: 10.1021/jp411948d.

[66] H. Gohlke and M. Thorpe. "A Natural Coarse Graining for Simulating Large Biomolecular Motion". In: *Biophysical Journal* 91.6 (2006), pp. 2115–2120. DOI: 10.1529/biophysj.106.083568.

[67] E. R. Davidson and D. Feller. "Basis set selection for molecular calculations". In: *Chemical Reviews* 86.4 (1986), pp. 681–696. DOI: 10.1021/cr00074a002.

[68] D Eberly. *Dynamic Collision Detection using Oriented Bounding Boxes*. https://www.geometrictools.com/Documentation/DynamicCollisionDetection.pdf. Accessed: 2017-01-12. Mar. 2008. URL: https://www.geometrictools.com/Documentation/DynamicCollisionDetection.pdf.

[69] S. Alfano and M. L. Greer. "Determining If Two Solid Ellipsoids Intersect". In: *Journal of Guidance, Control, and Dynamics* 26.1 (2003), pp. 106–110. DOI: 10.2514/2.5020.

[70] *MathNet.Numerics Package*. https://numerics.mathdotnet.com/. 2015. URL: https://numerics.mathdotnet.com/.

[71] *GNU Scientific Library Reference Manual - Third Edition*. Network Theory Ltd., Jan. 1, 2009. 592 pp. ISBN: 0954612078. URL: http://www.ebook.de/de/product/8165315/gnu_scientific_library_reference_manual_third_edition.html.

[72] W. E. Arnoldi. "The principle of minimized iterations in the solution of the matrix eigenvalue problem". In: *Quarterly of Applied Mathematics* 9.1 (1951), pp. 17–29. DOI: 10.1090/qam/42792.

[73] F. G. D. Sorensen. *ARPACK++, a C++ implementation of ARPACK eigenvalue package*. Center for Research on Parallel Computation, Rice University, Houston, Texas, EUA. 1997.

[74] Z.-Z. Yang and E. R. Davidson. "Evaluation of a characteristic atomic radius by an ab initio method". In: *International Journal of Quantum Chemistry* 62.1 (1997), pp. 47–53. DOI: 10.1002/(sici)1097-461x(1997)62:1<47::aid-qua5>3.0.co;2-3.

[75] R. A. Marcus. "Ion Pairing and Electron Transfer". In: *The Journal of Physical Chemistry B* 102.49 (1998), pp. 10071–10077. DOI: 10.1021/jp9834457.

[76] Y Shao. "Advances in molecular quantum chemistry contained in the Q-Chem 4 program package". In: *Molecular Physics* 113.2 (2014), pp. 184–215. DOI: 10.1080/00268976.2014.952696.

[77] V Rühle et al. "Microscopic Simulations of Charge Transport in Disordered Organic Semiconductors". In: *Journal of Chemical Theory and Computation* 7.10 (2011), pp. 3335–3345. DOI: 10.1021/ct200388s.

[78] J. Kirkpatrick. "An approximate method for calculating transfer integrals based on the ZINDO Hamiltonian". In: *International Journal of Quantum Chemistry* 108.1 (2007), pp. 51–56. DOI: 10.1002/qua.21378.

[79] J. Nelson. "Continuous-time random-walk model of electron transport in nanocrystallineTiO2electrodes". In: *Physical Review B* 59.23 (1999), pp. 15374–15380. DOI: 10.1103/physrevb.59.15374.

[80] T. Mori et al. "Quinoidal Naphtho[1,2-b:5,6-b′]dithiophenes for Solution-Processed n-Channel Organic Field-Effect Transistors". In: *Organic Letters* 16.5 (2014), pp. 1334–1337. DOI: 10.1021/ol5000567.

[81] S. Minami et al. "2,6-Diphenyl- and -distyryl-capped 3,7-dialkoxybenzo[1,2-b:4,5-b′]dithiophenes and their dithieno-annulated higher homologs: structural phase transition with enhanced charge carrier mobility". In: *Physical Chemistry Chemical Physics* 16.35 (2014), p. 18805. DOI: 10.1039/c4cp03002h.

[82] M. Nakano and K. Takimiya. "Sodium Sulfide-Promoted Thiophene-Annulations: Powerful Tools for Elaborating Organic Semiconducting Materials". In: *Chemistry of Materials* 29.1 (2017), pp. 256–264. DOI: 10.1021/acs.chemmater.6b03413.

[83] H Murata et al. "Non-dispersive and air-stable electron transport in an amorphous organic semiconductor". In: *Chemical Physics Letters* 339.3-4 (2001), pp. 161–166. DOI: 10.1016/s0009-2614(01)00306-2.

[84] D. Venkateshvaran. "Approaching disorder-free transport in high-mobility conjugated polymers". In: *Nature* 515.7527 (2014), pp. 384–388. DOI: 10.1038/nature13854.